National Institute
for Public Health
and the Environment

Letter report 680150004/2009

R.J. Wichink Kruit | A.P. Stolk | H. Volten | W.A.J. van Pul

NH_3 flux measurements at the micrometeorological weather station in Wageningen, The Netherlands

RIVM Letter report 680150004/2009

Flux measurements of ammonia at the micro-meteorological weather station in Wageningen, The Netherlands

R.J. Wichink Kruit
A.P. Stolk
H. Volten
W.A.J. van Pul

Contact:
R.J. Wichink Kruit
Centre for Environmental Monitoring (CMM)
National Institute for Public Health and the Environment (RIVM)
Roy.Wichink.Kruit@rivm.nl

This research is carried out on behalf of the Ministry of Housing, Spatial Planning and the Environment, Directorate General for Environmental Protection (VROM/DGM), in the framework of Project M/680150 Ammoniak.

RIVM Letter report 680150004/2009

Fluxmetingen van ammoniak op een micro-meteorologisch weerstation in Wageningen, Nederland

R.J. Wichink Kruit
A.P. Stolk
H. Volten
W.A.J. van Pul

Contact:
R.J. Wichink Kruit
Centrum voor MilieuMonitoring (CMM)
Rijks Instituut voor Volkgezondheid en Milieu (RIVM)
Roy.Wichink.Kruit@rivm.nl

Dit onderzoek werd verricht in opdracht van het ministerie van Volkshuisvesting, Ruimtelijke Ordening en Milieubeheer, Directoraat-Generaal Milieubeheer (VROM/DGM), in het kader van Project M/680150 Ammoniak.

Rapport in het kort

Fluxmetingen van ammoniak op een micrometeorologisch weerstation in Wageningen, Nederland.

Agrarisch grasland neemt aanzienlijk minder ammoniak uit de atmosfeer op dan tot nu tot werd aangenomen. Daardoor zit er in de atmosfeer een hogere concentratie ammoniak. Dit blijkt uit metingen op een micrometeorologisch weerstation in Wageningen door het RIVM en de Wageningen Universiteit. De metingen zijn boven agrarisch grasland verricht, dat 25 procent van het landareaal in Nederland omvat. Voorheen werden de metingen vooral in natuurgebied uitgevoerd. De komende jaren worden de consequenties van de nieuwe metingen in kaart gebracht. De metingen worden bovendien gebruikt om het transportproces van ammoniak van of naar het oppervlak beter te beschrijven.

Dit rapport beschrijft de metingen die aan deze conclusie ten grondslag liggen. Het onderzoek is uitgevoerd in opdracht van het ministerie van VROM, dat met deze metingen meer inzicht in de opname van ammoniak door grasland wilde hebben om het zogeheten ammoniakgat te verklaren. Het ammoniakgat is het verschil tussen de gemeten en berekende hoeveelheid ammoniak in de lucht, en is mede door dit onderzoek niet meer significant.

Ammoniak komt voornamelijk in de atmosfeer terecht door verdamping uit mest in stallen en bij het uitrijden van mest over het land. De hoeveelheid ammoniak die planten en de bodem opnemen is van invloed op de hoeveelheid ammoniak in de atmosfeer.

Abstract

Flux measurements of ammonia from a micro-meteorological weather station in Wageningen, the Netherlands.

Agricultural grassland absorbs considerably less ammonia from the atmosphere than has been believed up until now. This means that there is a higher concentration of ammonia in the atmosphere. This can be concluded from measurements taken from a micro-meteorological weather station in Wageningen by researchers from the National Institute for Public Health and the Environment (RIVM) and Wageningen University. The measurements were taken above agricultural grassland that covers 25 percent of the total land area of the Netherlands. In the past, the measurements were taken especially in nature areas. The consequences of the new measurements will be documented in future years. Moreover, the measurements will be used in particular, to describe the transport process of ammonia to or from the surface.

This report describes the measurements on which this conclusion has been based. Commissioned by the Ministry of Spatial Planning and the Environment (VROM), the study was conducted to gain more insight in the uptake of ammonia through grassland in order to explain the so-called ammonia gap in the Netherlands. The ammonia gap is the difference between the measured and the calculated amount of ammonia which (partly due to the results of this study) is no longer significant.

Ammonia enters the atmosphere especially through the process of evaporation from manure in animal stalls and when liquid manure is spread over the land. The amount of ammonia absorbed by plants and the soil influences the amount of ammonia in the atmosphere.

Contents

Summary

To improve the description of the dry deposition process, new measurements of ammonia fluxes over agricultural grassland have been carried out by the National Institute for Public Health and the Environment (RIVM) in cooperation with the department of Meteorology and Air Quality of Wageningen University. The measurements with the new measurement device, the Gradient Ammonia – High Accuracy – Monitor (GRAHAM; Wichink Kruit et al., 2007), started in June 2004 and ended in December 2006. The GRAHAM, the measurement technique, the measurement site, the uncertainties in the measurements and the measurements themselves are described in this report.

After correction for the known systematic errors in the concentration measurements, a relative random error in the concentration of 1.9% is found. The relative random error in the NH_3 flux measurements (mainly determined by the propagation of the random errors in the concentration measurements in the flux calculation) is on average 52% (with a median value of 31%). If we would not correct for the systematic errors in the concentration measurements (0.6%), we would have an average systematic error in the flux calculation of 18%. This means that the systematic error is relatively small compared to the random error of the flux measurements on an hourly basis.

The measurements showed that the surface resistance (R_c), in particular the cuticular resistance (R_w), to uptake of ammonia was much larger than assumed in the DEPAC (deposition) module used in the OPS model of RIVM and PBL and the Lotos/Euros model of TNO, RIVM and PBL. The currently applied resistance parameterisations for the dry deposition of ammonia on agricultural grassland are mainly based on measurements over natural ecosystems or semi-natural grasslands in areas with low ambient ammonia concentrations. We have shown in this report that the relatively high background concentrations in this study lead to higher surface resistances (and consequently lower deposition velocities) over agricultural grassland in The Netherlands. This is in agreement with findings of higher R_w values for different vegetations in high background concentration areas in literature (Nemitz et al., 2001).

The main conclusion of this report is that the dry deposition description in the DEPAC module should be updated according to the current knowledge.

This research project is part of the research carried out to explain the ammonia gap in the Netherlands (van Pul et al., 2008).

1 Introduction

Several processes determine and influence the ammonia cycle in the atmosphere. Figure 1 shows the atmospheric processes that are important for ammonia. It starts with the *emission* of ammonia (red arrow in Figure 1). In The Netherlands, it was estimated that a total of 0.133 Tg of NH_3 (= 133 kton) was emitted in 2004 (Milieubalans, 2007), of which about 90% was of agricultural origin. For comparison, the yearly global emission was about 45 Tg NH_3, of which about 67% was of agricultural origin (Dentener and Crutzen, 1994).

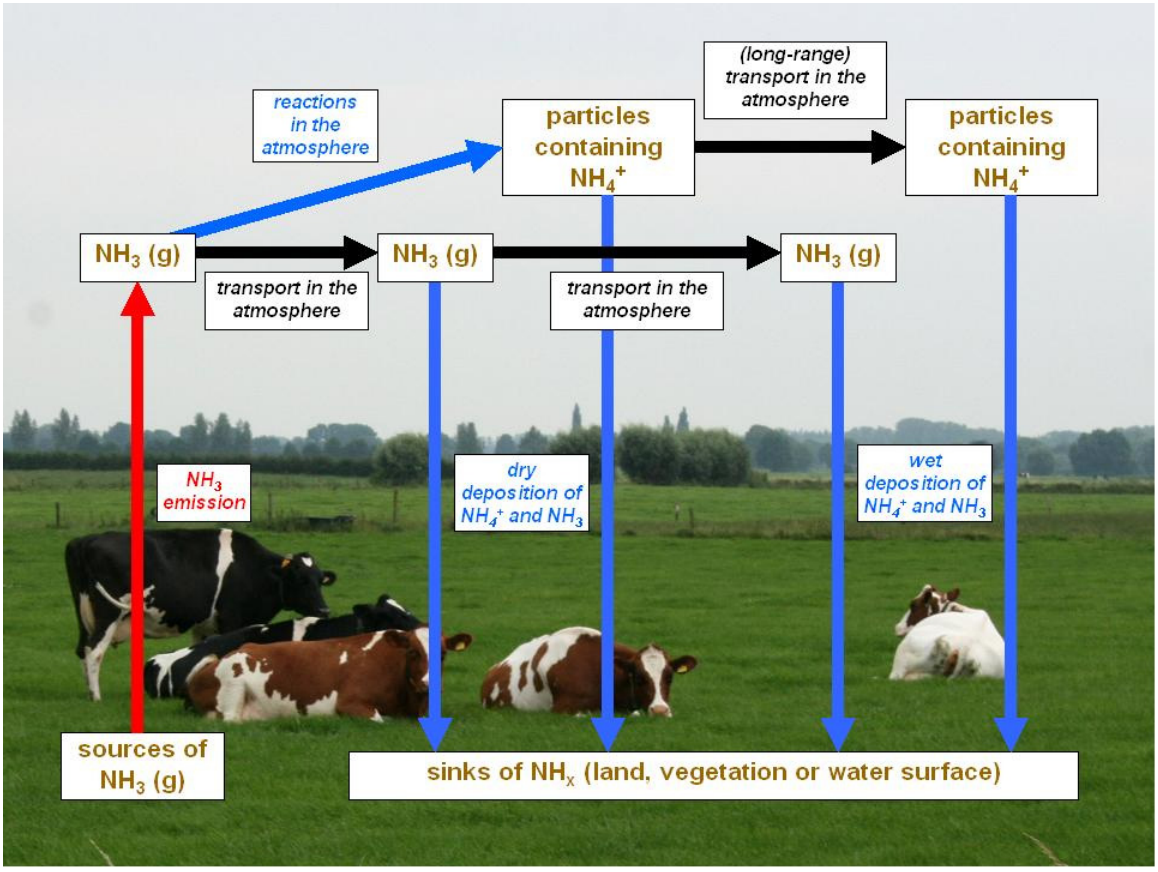

Figure 1. Ammonia flows in the atmosphere.

Emission of NH_3 is followed by *atmospheric transport* (black arrows in Figure 1). Transport and dispersion of ammonia in the atmosphere occurs by mean wind and turbulence.
There are three removal mechanisms for ammonia (blue arrows in Figure 1):

- The first one is *chemical reactions* that transform ammonia gas into particles containing ammonium. These particles have a longer lifetime than ammonia gas and are therefore transported over much larger distances.
- The second removal mechanism is *dry deposition* of NH_3 and NH_4^+. NH_3 and NH_4^+ are absorbed by soil, vegetation and water surfaces. Dew plays an important role in the dry deposition process by enhanced surface wetness, because ammonia is well soluble in water.

- The third removal mechanism is *wet deposition*. Wet deposition is the transfer of NH_3 and NH_4^+ to the ground via precipitation, e.g. rain and snow. Wet deposition measurements are usually directly estimated from the measurement of the concentrations in precipitation and precipitation amount.

One of the main items in the air pollution policy of the Dutch government is to reduce agricultural ammonia emissions. Over the last 30 years, ammonia has become widely recognized as a major atmospheric pollutant as a result of the effects of its deposition onto terrestrial and aquatic ecosystems and its influence on regional scale tropospheric chemistry (Grennfelt et al., 1994; Derwent et al., 1988). Deposition of reactive and reduced nitrogen species induces shifts in the nutrient balance that intensifies the eutrophication process. As a consequence, the existence of plant species changes and a loss of biodiversity occurs. Ammonia also contributes to the acidification of ecosystems through microbial oxidation (nitrification) in the soil. Therefore, the quantification of ammonia deposition is of great interest in assessing the effects of nitrogen loading to ecosystems.

To monitor the effectiveness of the measures taken by the government, The National Institute for Public Health and the Environment (RIVM, Bilthoven, The Netherlands) measures ammonia concentrations at 8 locations around the country and combines them with model calculations with an atmospheric transport model (OPS; Van Jaarsveld, 2004) to get a representative map of the ammonia concentrations and the ammonia deposition over the Netherlands.

The yearly averaged ammonia concentration observed by the monitoring network is plotted in Figure 2 (black solid line with squares). The figure also shows the total ammonia emissions by agricultural and other sources (bars), and the modelled ammonia concentration by the OPS model (red dashed line with triangles). A significant reduction in the emissions of ammonia is observed between 1993 (0.233 Tg yr^{-1}) and 2002 (0.139 Tg yr^{-1}). The measured yearly averaged ammonia concentration follows the decrease in ammonia emissions (from 10.6 µg m^{-3} in 1993 to 7.2 µg m^{-3} in 2002).

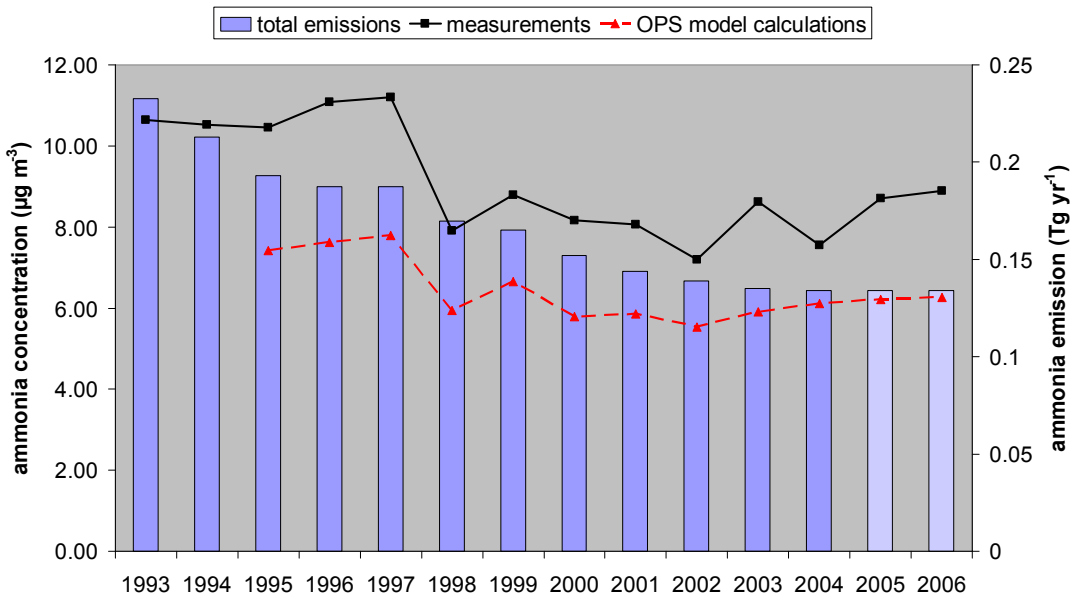

Figure 2. Emission, measured and modelled ammonia concentration from 1993 till 2006 (van Pul et al., 2008).

In general, the modelled concentrations (red dashed line with triangles) are lower than the measured concentrations (black solid line with squares). This absolute difference between the measured and modelled ammonia concentrations is about 30% and is called the '*ammonia gap*'. Research on the 'ammonia gap' focuses on improving the *emission factors* from manure application (Berkhout et al., 2008) and improving the description of the *dry deposition process*. This report focuses on the latter.

The dry deposition process is the most important removal process for ammonia from the atmosphere, however, it is usually not measured directly. The dry deposition flux is estimated as the product of the measured ammonia concentration (μg m^{-3}) and a modelled deposition velocity (m s^{-1}). The modelled deposition velocities at the ecosystem scale are based on process-based exchange models (Jakobsen et al., 1997). Much work has already been done to provide a mechanistic understanding of processes regulating the exchange (Sutton et al., 1993), however, there remain large uncertainties in these flux estimates, as there is a lack of validation by both laboratory and field measurements, especially over agricultural surfaces. However, for the mass balance (or concentration), ammonia exchange with especially agricultural grassland is very important as it covers about 25% of all land surface in The Netherlands.

To evaluate the existing parameterisation for the exchange of ammonia with agricultural grassland in the OPS model (Van Jaarsveld, 2004), measurements of ammonia fluxes over agricultural grassland have been carried out by RIVM in cooperation with the department of Meteorology and Air Quality of Wageningen University. The measurements of NH_3 exchange started in June 2004 and ended in December 2006. Non-fertilized grassland was chosen as a target land cover type as it is assumed to be useful as a background situation for all the (intensively) managed grasslands in The Netherlands.

In this report the measurements above the grassland at the Haarweg, The Netherlands are presented. The first part of the report focuses on the theory and the methods applied. In Chapter 2 it is presented how the fluxes are derived from concentration measurements and how reliable data are selected from the dataset. Chapter 3 provides details about the measurement site and the instrumentation used to derive the ammonia fluxes. Chapter 4 presents an error analysis to give an impression of the errors in the concentration as well as in the flux measurements.
The second part of the report focuses on the results. In Chapter 5, an overview of the collected data and derived variables is shown. In Chapter 6, these results are discussed and placed in an international perspective.

The results of this research have been used in the report on the status of the ammonia gap (Van Pul et al., 2008)

2 Derivation of the flux

This chapter describes how the flux can be derived from concentration gradient and micrometeorological measurements. The gradient (or flux-profile) technique is commonly used in dry deposition studies and is based on the theory of turbulent flow of the atmospheric boundary layer. In applying this technique one should keep in mind that it is based on theory, which is only valid under certain conditions. If these conditions are not met this will lead to serious errors in the estimated flux.

2.1 Basic theory

Starting with the basic conservation equation of ammonia and expanding into mean ($\bar{\chi}$) and turbulent (χ') parts, the following equation is obtained (e.g. Stull, 1988):

$$\frac{\partial\bar{\chi}}{\partial t}+\frac{\partial\chi'}{\partial t}+\frac{\overline{U_j}\partial\bar{\chi}}{\partial x_j}+\frac{\overline{U_j}\partial\chi'}{\partial x_j}+\frac{u_j'\partial\bar{\chi}}{\partial x_j}+\frac{u_j'\partial\chi'}{\partial x_j}=\frac{D\partial^2\bar{\chi}}{\partial x_j^{\,2}}+\frac{D\partial^2\chi'}{\partial x_j^{\,2}}+S \qquad (1)$$

where χ is the ammonia concentration, t is time, U is wind speed, x is the direction, u' is wind speed fluctuation, D is the molecular diffusivity of ammonia, S is the net remaining source/sink term and j indicates the three spatial dimensions (x, y and z). Reynolds averaging and using the turbulent continuity equation (which puts the turbulent advection term into flux form (term III)) gives:

$$\underbrace{\frac{\partial\bar{\chi}}{\partial t}}_{I}+\underbrace{\frac{\overline{U}\partial\bar{\chi}}{\partial x}+\frac{\overline{V}\partial\bar{\chi}}{\partial y}+\frac{\overline{W}\partial\bar{\chi}}{\partial z}}_{II}+\underbrace{\frac{\partial\left(\overline{u'\chi'}\right)}{\partial x}+\frac{\partial\left(\overline{v'\chi'}\right)}{\partial y}+\frac{\partial\left(\overline{w'\chi'}\right)}{\partial z}}_{III}=\underbrace{\frac{D\partial^2\bar{\chi}}{\partial x^2}+\frac{D\partial^2\bar{\chi}}{\partial y^2}+\frac{D\partial^2\bar{\chi}}{\partial z^2}}_{IV}+\underbrace{S}_{V} \qquad (2)$$

Term I represents the mean storage of ammonia (i.e. concentration change in time).
Term II describes the advection of ammonia by the mean wind.
Term III represents the divergence of the ammonia flux.
Term IV represents the mean molecular diffusion of ammonia.
Term V is the mean net body source (or sink) term for additional ammonia processes.
where U, V and W (and u, v and w) are the wind speed (fluctuations) in the x, y and z direction respectively.

To investigate the relative importance of each term in Equation 2, we scale all variables (a) with a typical scale (A) to make them dimensionless (â). We replace all variables according to â = a / A and Equation 2 is then rewritten as:

$$\underbrace{\frac{C}{t}\left[\frac{\partial\hat{\bar{\chi}}}{\partial\hat{t}}\right]}_{I}+\underbrace{\underbrace{\frac{V_x\Delta c_x}{L}\left[\frac{\overline{\hat{U}}\partial\hat{\bar{\chi}}}{\partial\hat{x}}\right]}_{IIA}+\underbrace{\frac{V_y\Delta c_y}{B}\left[\frac{\overline{\hat{V}}\partial\hat{\bar{\chi}}}{\partial\hat{y}}\right]}_{IIB}+\underbrace{\frac{V_z\Delta c_z}{Z}\left[\frac{\overline{\hat{W}}\partial\hat{\bar{\chi}}}{\partial\hat{z}}\right]}_{IIC}}_{II}+$$

$$\underbrace{\underbrace{\frac{v_x c}{L}\left[\frac{\partial\left(\overline{\hat{u}'\hat{\chi}'}\right)}{\partial\hat{x}}\right]}_{IIIA}+\underbrace{\frac{v_y c}{B}\left[\frac{\partial\left(\overline{\hat{v}'\hat{\chi}'}\right)}{\partial\hat{y}}\right]}_{IIIB}+\underbrace{\frac{v_z c}{Z}\left[\frac{\partial\left(\overline{\hat{w}'\hat{\chi}'}\right)}{\partial\hat{z}}\right]}_{IIIC}}_{III}= \qquad (3)$$

$$\underbrace{\underbrace{\frac{DC}{L^2}\left[\frac{D\partial^2\hat{\bar{\chi}}}{\partial\hat{x}^2}\right]}_{IVA}+\underbrace{\frac{DC}{B^2}\left[\frac{D\partial^2\hat{\bar{\chi}}}{\partial\hat{y}^2}\right]}_{IVB}+\underbrace{\frac{DC}{Z^2}\left[\frac{D\partial^2\hat{\bar{\chi}}}{\partial\hat{z}^2}\right]}_{IVC}}_{IV}+\underbrace{S\left[\hat{S}_\chi\right]}_{V}$$

Note that all factors between brackets are dimensionless and have values in the order of unity. The factors before the brackets are the scale variables needed to make the variables dimensionless. In Table 1 characteristic scales for all scale variables in Equation 3 are defined to investigate the relative importance of the individual terms.

Table 1. Characteristic scales and typical values used in scaling of the conservation equation of the concentration of ammonia.

Characteristic scale	Symbol	Typical value
concentration scale for NH_3	C	10 μg m^{-3}
concentration fluctuation scale for NH_3	c	1 μg m^{-3}
concentration difference scales for NH_3 in the x, y and z direction	Δc_x, Δc_y, Δc_z	1, 1, 10 μg m^{-3}
time scale of the mean concentration change of NH_3	t	10000 s
mean wind speed scales of U, V and W	V_x, V_y, V_z	5, 5, 0.001 m s^{-1}
wind fluctuation scales in x, y and z direction	v_x, v_y, v_z	2, 2, 1 m s^{-1}
length scales in the x, y and z direction	L, B, Z	200, 200, 4 m
molecular diffusion coefficients for NH_3	D	1.8 10^{-5} m^2 s^{-1}

If we fill in the typical values for the scales from Table 1 in Equation 3, we are able to make an estimation of the importance of each term:

I local time derivative:

$$\frac{C}{t} = \frac{10}{10000} = 0.001$$

IIA and IIB advection by mean flow:

$$\frac{V_x \Delta c_x}{L} = \frac{5 \cdot 1}{200} = 0.025$$

IIC convection by mean flow:

$$\frac{V_z \Delta c_z}{Z} = \frac{0.001 \cdot 10}{4} = 0.0025$$

IIIA and IIIB advection by turbulence:

$$\frac{v_x c}{L} = \frac{2 \cdot 1}{200} = 0.01$$

IIIC convection by turbulence:

$$\frac{v_z c}{Z} = \frac{1 \cdot 1}{4} = 0.25$$

IVA and IVB molecular diffusion:

$$\frac{DC}{L^2} = \frac{10 \cdot 1.8 \times 10^{-5}}{200^2} = 4.5 \times 10^{-9}$$

IVC molecular diffusion:

$$\frac{DC}{Z^2} = \frac{10 \cdot 1.8 \times 10^{-5}}{4^2} = 1.125 \times 10^{-5}$$

As we do not have any information about the source/sink term (V), this term is ignored. However, it seems unlikely that sources and sinks are very strong within the surface layer and therefore this term is assumed to be relatively small compared to the other terms. We have to keep in mind that ignoring term V does not mean that there is no source or sink at the surface itself. We only ignore sources or sinks within the surface layer (e.g. chemical conversions within the surface layer).

We see that the largest term in Equation 3 is the convection by turbulence term (IIIC) and that all other terms are at least one order of magnitude smaller. Therefore, as an approximation, Equation 2 is reduced to $\frac{\partial\left(\overline{w'\chi'}\right)}{\partial z} \approx 0$, which means that the flux is approximately constant with height. In other words, the flux that is measured at a certain height is approximately the same as the flux at the surface. The second largest term in Equation 3 is the advection by mean flow term (IIA and IIB). To be sure that the derived fluxes are not influenced by advection, we will use footprint analysis (Chapter 2.3) to exclude situations that advection might influence the flux measurements.

2.2 Gradient or flux-profile technique

At present, there exists no operational fast response sensor for ammonia. As a consequence, the ammonia fluctuations, χ', cannot be measured and the ammonia flux, $F_\chi = -\left(\overline{w'\chi'}\right)$, can not be derived directly.
Therefore, we have to rely on another method to derive the ammonia flux: the gradient or flux-profile technique. This method relates the flux of ammonia to the vertical gradient of ammonia analogous to the description of molecular diffusion by Fick's law:

$$F_\chi = -K_\chi \frac{\partial \bar{\chi}}{\partial z} \tag{4}$$

where $\partial\chi/\partial z$ is the concentration gradient, i.e. the concentration difference, $\partial\chi$, over a height difference, ∂z, and K_χ is the eddy diffusion coefficient for ammonia. K_χ is a property of the flow and depends largely on turbulence in that flow.

Characteristic turbulence scales for the different scalar quantities are defined: a turbulence velocity scale, the so-called friction velocity:

$$u_* = \left(\overline{u'w'}^2 + \overline{v'w'}^2\right)^{1/4} \tag{5a}$$

and a turbulence scale for the quantity of interest such as temperature, absolute humidity or in our case ammonia (χ), generally written as:

$$\chi_* = -\frac{\overline{w'\chi'}}{u_*} \tag{5b}$$

By combining Equation 5a and 5b, the ammonia flux is written as:

$$F_\chi = -u_*\chi_* \tag{6}$$

The gradient in Equation 4 is made dimensionless through the flux-profile relationships (or stability functions) for ammonia (Φ_χ), which is assumed to be transported in the same way as heat (H) and moisture (Q), e.g. $\Phi_\chi(\zeta) \approx \Phi_H(\zeta) \approx \Phi_Q(\zeta)$ (Dyer and Hicks, 1970; Businger et al., 1971; Webb, 1980):

$$\frac{kz}{u_*}\frac{\partial \bar{U}}{\partial z} = \Phi_m(\zeta) \tag{7a}$$

$$\frac{kz}{\chi_*}\frac{\partial \bar{\chi}}{\partial z} = \Phi_\chi(\zeta) \approx \Phi_H(\zeta) \tag{7b}$$

where k is the von Karman's constant (=0.4). The dimensionless flux-profile relationships Φ_m and Φ_χ are functions of the atmospheric stability parameter $\zeta = z/L$, where L is the Obukhov length scale defined by:

$$L = -\frac{T}{kg}\frac{u_*^3}{\overline{w'\chi'}} \tag{8}$$

Using Equation 4, 6 and 7, the eddy diffusion coefficient for ammonia is written as:

$$K_\chi = \frac{k u_* z}{\Phi_\chi(\zeta)} \tag{9}$$

If we integrate Equation 7a over a height difference, z - $z_{0,m}$, we obtain:

$$\int_{z_{0,m}}^{z} \partial\overline{U} = \int_{z_{0,m}}^{z} \frac{u_*\Phi_m(\zeta)}{kz}\partial z \equiv \overline{U}(z) - \overline{U}(z_{0,m}) = \frac{u_*}{k}\left(\ln\left(\frac{z}{z_{0,m}}\right) - \Psi_m\left(\frac{z}{L}\right) + \Psi_m\left(\frac{z_{0,m}}{L}\right)\right) \tag{10a}$$

In a similar way Equation 7b is integrated over a height difference, z - $z_{0,\chi}$:

$$\overline{\chi}(z) - \overline{\chi}(z_{0,\chi}) = \frac{\chi_*}{k}\left[\ln\left(\frac{z}{z_{0,\chi}}\right) - \Psi_\chi\left(\frac{z}{L}\right) + \Psi_\chi\left(\frac{z_{0,\chi}}{L}\right)\right] \tag{10b}$$

where $\psi_m(\zeta)$ and $\psi_\chi(\zeta)$ are the integrated stability functions, $z_{0,m}$ and $z_{0,\chi}$ are the characteristic length scales of the underlying surface for wind velocity, U, and ammonia, χ, respectively. They indicate the height above a virtual zero level at which the centre is located where the quantity is transmitted, absorbed or released. The $z_{0,m}$, called the roughness length, is dependent on the roughness of the surface. The $z_{0,\chi}$ is mainly dependent on the vertical distribution of the sources or sinks of ammonia at the surface.

Here, we use the integrated stability functions of Paulson (1970) and Dyer (1974) for unstable conditions (i.e. L < 0):

$$\Psi_m(\zeta) = 2\ln\left[\frac{1+x}{2}\right] + \ln\left[\frac{1+x^2}{2}\right] - 2\tan^{-1}(x) + \frac{\pi}{2} \tag{11a}$$

$$\Psi_\chi(\zeta) \approx \Psi_H(\zeta) = 2\ln\left[\frac{1+x^2}{2}\right] \tag{11b}$$

where $x = (1-16\zeta)^{1/4}$ with $\zeta = z/L$

and the integrated stability functions of Beljaars and Holtslag (1991) for stable conditions (i.e. L > 0):

$$\Psi_m(\zeta) = -a\zeta - b\left(\zeta - \frac{c}{d}\right)\exp(-d\zeta) - \frac{bc}{d} \tag{12a}$$

$$\Psi_\chi(\zeta) \approx \Psi_H(\zeta) = -\left(1 + \frac{2}{3}a\zeta\right)^{3/2} - b\left(\zeta - \frac{c}{d}\right)\exp(-d\zeta) - \frac{bc}{d} + 1 \tag{12b}$$

where a = 1, b = 0.667, c = 5, d = 0.35 and $\zeta = z/L$.

Substituting Equation 10a and 10b into Equation 6 provides an expression for the ammonia flux as:

$$F_\chi = -\frac{k\left[\overline{U}(z) - \overline{U}(z_{0,m})\right]}{\left[\ln\left(\frac{z}{z_{0,m}}\right) - \Psi_m\left(\frac{z}{L}\right) + \Psi_m\left(\frac{z_{0,m}}{L}\right)\right]}\frac{k\left[\overline{\chi}(z) - \overline{\chi}(z_{0,\chi})\right]}{\left[\ln\left(\frac{z}{z_{0,\chi}}\right) - \Psi_\chi\left(\frac{z}{L}\right) + \Psi_\chi\left(\frac{z_{0,\chi}}{L}\right)\right]} \tag{13}$$

However, for the flux measurements presented in this report, u_* was obtained directly from eddy covariance measurements using a sonic anemometer rather than from wind speed profiles. The vertical concentration gradients are measured by the GRadient Ammonia – High Accuracy – Monitor

(GRAHAM, described elsewhere). Consequently, the ammonia flux was found from the following expression:

$$F_\chi = -ku_* \frac{\left[\bar{\chi}(z) - \bar{\chi}(z_{0,\chi})\right]}{\left[\ln\left(\frac{z}{z_{0,\chi}}\right) - \Psi_\chi\left(\frac{z}{L}\right) + \Psi_\chi\left(\frac{z_{0,\chi}}{L}\right)\right]} \tag{14}$$

Because several measuring heights are available, the quotient is calculated from linear regression through the concentration differences (numerator) and the stability corrected heights (denominator).

2.3 Footprint analysis

The validity of the above flux measurement method relies on the principle of the flux being constant with height. However, this is only true for the surface layer in equilibrium with a homogeneous surface. Changes in the roughness of a surface or in the vegetative properties will lead to changes in the vertical flux. To ensure that the flux measurement is representative for a particular surface, the measurement height must be within the new internal boundary layer which forms after a surface inhomogeneity (which might be a local source or sink). The height of this layer (δ) depends on the upwind distance (x_L) or "fetch" to the inhomogenity. Empirical evidence suggests that the ratio of x_L to δ is approximately 100:1 (Monteith and Unsworth, 1990). However, the extent of an upwind area affecting a flux measurement changes with wind direction, wind speed, surface roughness and stability. Therefore, a more thorough analysis has been developed to assess the contribution to the flux measurement from a particular upwind source area, this is termed "footprint" analysis. The footprint is defined as "the upwind area most likely to affect a downwind flux measurement at a given height z" (Schuepp et al., 1990). Schuepp et al. (1990) provided analytical solutions of the diffusion equation based on Gash (1986) and defined the Cumulative Normalized contribution to the Flux measurement (CNF) at height z and upwind distance x_L. To account for non-neutrality Schuepp et al. (1990) also proposed an approximate adjustment by multiplying by the momentum stability correction function (Φ_m) resulting in:

$$\mathrm{CNF}(x_L) = \exp\left(-\frac{U \cdot z}{ku_* x_L}\Phi_m\left(\frac{z}{L}\right)\right) \tag{15}$$

where U is defined as the average wind speed between the surface and the measurement height z, assuming a logarithmic wind speed profile for neutral stability:

$$U = \frac{\int_{z_0}^{z} u(z)dz}{\int_{z_0}^{z} dz} = \frac{u_*\left[\ln\left(\frac{z}{z_0}\right) - 1 + \left(\frac{z_0}{z}\right)\right]}{k\left(1 - \left(\frac{z_0}{z}\right)\right)} \tag{16}$$

If this equation is substituted in Equation 15, the following equation for the CNF is obtained:

$$\mathrm{CNF}(x_L) = \exp\left(-\frac{\left[\ln\left(\frac{z}{z_0}\right) - 1 + \left(\frac{z_0}{z}\right)\right]z}{k^2\left(1 - \left(\frac{z_0}{z}\right)\right)x_L} \cdot \Phi_m\left(\frac{z}{L}\right)\right) \tag{17}$$

Figure 3 shows the CNF as a function of x_L for different measuring heights (z) and different stabilities (stable (L = 5), unstable (L = - 5) and neutral (L = ± ∞)). Here, we used U/u_* of 12.2 for 4 meters height and 8.8 for 1 meter height (derived from measurements). The figure shows that as long as the measurements are carried out close to the ground, even in very stable situations, the measurements mainly 'see' their direct environment. However, especially in very stable situations, a high measuring height leads to small CNF values (or in other words, a high measuring height is influenced by a larger surrounding especially in stable situations).

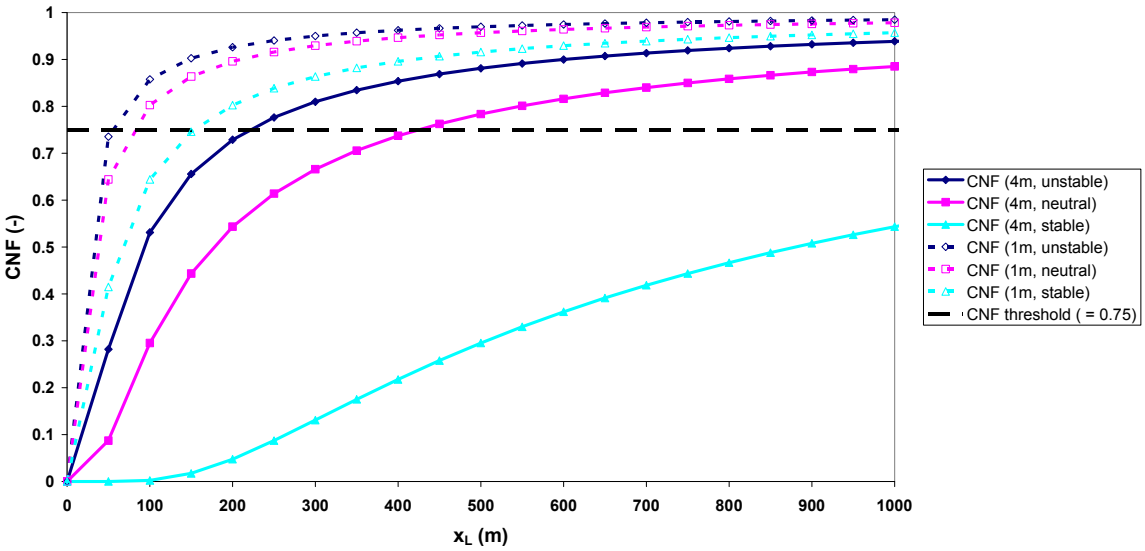

Figure 3. CNF for various values of measurement height and stability as a function of x_L.

Monteith and Unsworth (1990) proposed a typical ratio between measurement height and fetch of 1:100 for short vegetation. In neutral conditions, the fetch for a measurement height of 4 metres should then be at least 400 metres, which corresponds to a CNF threshold of 0.75 (the black dashed line in Figure 3). We will also apply this CNF threshold to stable and unstable conditions, which means that the required fetch increases to at least 2100 m in stable conditions (L = 5 m) and reduces to at least 225 m in unstable condition (L = -5 m).

3 Site description and instrumentation

3.1 Site description

All reported NH_3 flux measurements are calculated from concentration profiles measured at a meteorological observatory, where continuous measurements of air and soil temperature, air humidity, radiation, wind direction and wind speed are available. The measurement site is located west of Wageningen in The Netherlands (51° 58' 18" N; 5° 38' 30" E) on a heavy clay soil with a temperate humid perennial ryegrass pasture (*Lolium perenne*) (Van Hove, 1989). Figure 4 shows an aerial overview of the meteorological observatory and its surroundings. The black dot represents the location of the ammonia gradient set-up. There is no application of manure at the site and grass is cut on average 3-4 times a year. The average elevation of the measurement site is 6.80m above mean sea level. (Webpage of observatory: http://www.maq.wur.nl).

Figure 4. Aerial view of the micrometeorological site 'Haarweg' in Wageningen, The Netherlands. (courtesy: Google Earth)

3.2 Instrumentation

3.2.1 Meteorological instrumentation

The micrometeorological weather station at the Haarweg in Wageningen is a Special Agro-Meteorological Station. Appendix A gives an overview of the standard (micro)meteorological variables that are measured at this observatory. Besides these standard meteorological variables, measurements of horizontal wind speed (U), wind direction, friction velocity (u_*) and sensible heat flux (H) are provided by a CSAT3 3-D sonic anemometer (Campbell Scientific) mounted at 3.5 m.
Meteorological variables are logged with a frequency of once every 10 minutes. The micrometeorological flux measurements, however, are averaged over a 30-minute time period. Since these data are required for the eventual ammonia flux calculations, all measurements are converted to 30-minute averages.

3.2.2 Ammonia instrumentation

The NH_3-concentration profiles (needed in Eq. 14) are measured using the new GRadient Ammonia – High Accuracy – Monitor (GRAHAM), a more advanced version of the AMANDA (a continuous rotating wet denuder analyzer; Wyers et al., 1993; Wichink Kruit et al., 2007). The GRAHAM (shown in Figure 5) is an instrument that measures the NH_3-concentration at 1 m, 2.5 m (2.0 m from 30 May 2005 onwards) and 4 m height with a frequency of once every 10 minutes. The GRAHAM is well suited for micrometeorological measurements because of its low detection limit, high precision and accuracy and high time resolution. The measurement principle of the GRAHAM denuder is basically the same as the existing AMANDA denuder as described by Wyers et al. (1993, 1998).

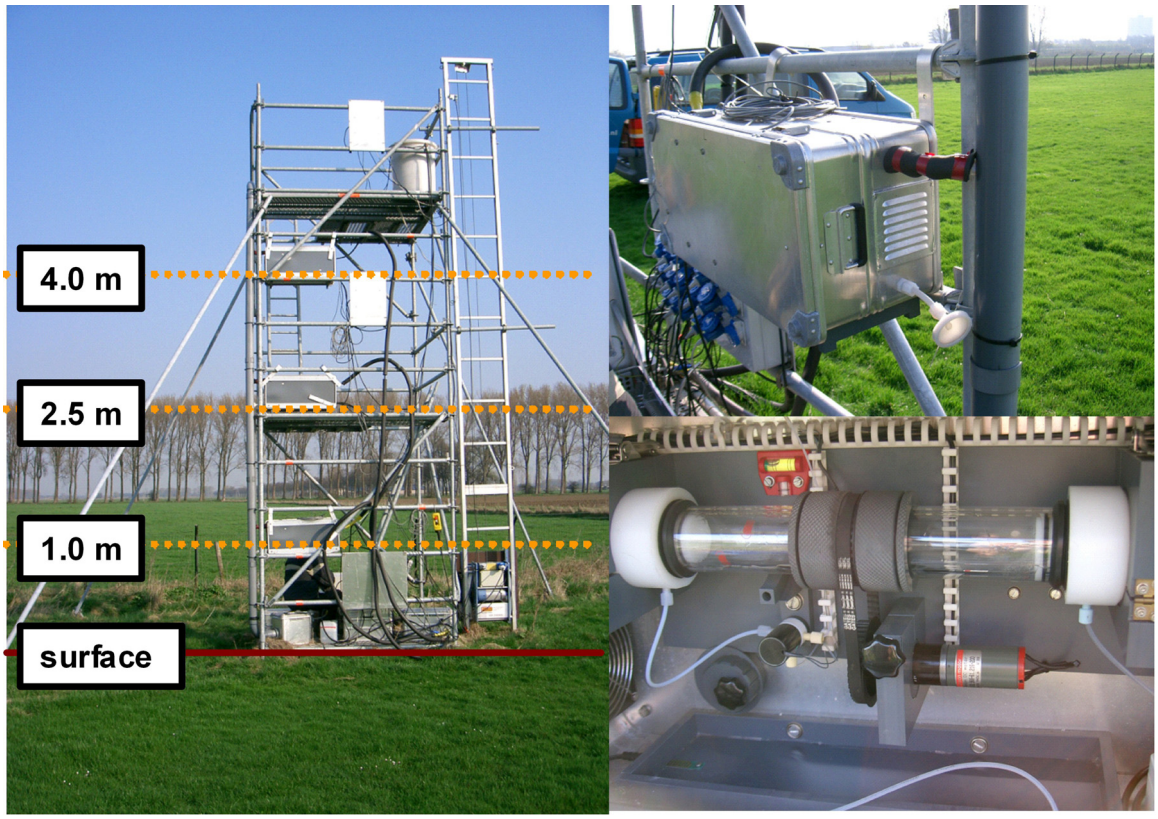

Figure 5. GRAHAM measurement system (left), close up of one of the three denuder boxes (upper right) and close up of an annular denuder inside the box (lower right).

The GRAHAM uses horizontally-positioned rotating annular denuder tubes. A denuder tube consists of two concentric glass tubes of 30 cm in length and up to 50 mm in diameter. The walls of the annular denuder are coated with a slightly acidic absorption fluid (3.6 mM $NaHSO_4$). Air is pumped through the space between the two glass tubes at a rate of approximately 23 l min^{-1}. Any gaseous ammonia present in the air diffuses to the walls of the denuder, where it is captured by the absorption fluid. Ammonium aerosol (NH_4^+) passes through the denuder almost unimpeded (only 1-2% absorption) as the diffusion rate of aerosols is much smaller than that of the gaseous NH_3.
The absorption fluid is continuously pumped through the denuders at a rate of 1 ml min^{-1} and flows in opposite direction to the air flow. The absorption fluid containing the dissolved NH_3 (as NH_4^+) is now analyzed by a common detector. Once in the detector, the absorption fluid containing NH_4^+ is mixed with a solution of 0.5 M NaOH, so that molecular ammonia is formed again. This molecular ammonia diffuses through a semi-permeable PTFE membrane and is dissolved in de-ionized water present on the other side of the membrane. At pH lower than 7, it is mostly present in the form of NH_4^+ and the NH_4^+ concentration in this water flow is determined by conductivity. The analyzer is calibrated with aqueous standards of typically 0, 50 and 500 µg l^{-1} NH_4^+. The detection limit of NH_3 in air is approximately 0.02 µg m^{-3}.
Several modifications have been carried out with respect to the AMANDA to improve the accuracy as well as the precision of the instrument. In the old AMANDA system flow rates were determined manually at service visits. In the current GRAHAM system continuous in-line airflow measurements are implemented, which is an obvious improvement with respect to the precision and accuracy. The

flow rates are determined by measurements of temperature and the pressure drop over a restriction. To minimize systematic errors the restrictions have been brought together in an aluminium body.
Second, two 3-channel syringe pumps (type Mechatronics) replaced the multi channel peristaltic pump allowing a well-defined sample flow from the denuders. With two coupled 10 ml syringes per denuder and a 1 ml min^{-1} sample flow a cycle time of ten minutes is obtained. During a cycle time the three samples are sequentially led through the detector allowing two minutes of flushing in between.
Third, the conical structure in the inlet is now also applied on the outlet of the wet rotating denuder. This optimized aerosol conducting system prevents ammonium containing particles (aerosols) from impaction on wetted surfaces and from being a potential source of interfering ammonium.
Average concentration values for all three denuders were determined during a 10 minute cycle. The 3 denuders were sampled sequentially with a stabilizing time of 2 minutes and an averaging time of 1 minute. After this cycle of 9 minutes, the detector is flushed for 1 minute and a new cycle starts. The tube length for transporting the solution to the detector is equal for all three heights to ensure that the concentrations measured in the analyzer refer to identical air sampling periods.
A vertical PVC pipe of diameter 0.1 m was attached to the three denuders to be able to mutually compare the three denuders in the field. A high volume of ambient air is blown through the pipe (about 200 m^3 hr^{-1}) to ensure that the concentration at all three denuder heights is the same during comparison. Each denuder samples the same air from this PVC pipe and should consequently measure the same concentration. Observed differences between the individual denuders can be considered as systematic differences. With this vertical PVC pipe, we are able to correct for the systematic differences between the denuders under field conditions. The procedure for systematic error correction is described in the following chapter.

4 Error analysis

4.1 Systematic and random errors in the concentration

4.1.1 Laboratory comparison

Data on the performance of the earlier version of this instrument (AMANDA) were reported by Wyers et al. (1993, 1998) and Mennen et al. (1996). Wyers et al. (1993) positioned three instruments in the field at the same height and averaged the measurements every 30 min. They corrected the obtained concentrations for systematic differences, and reported the between-instrument standard deviation based upon 22 simultaneous triplicates to be 2.6% relative over the entire time spanned by the concentrations. The correction method and the concentrations themselves were not reported. The current GRAHAM system was tested in a similar way. The three instruments were placed on a lab bench. They were simultaneously fed with the same sample, which was alternately clean air and 8 µg m^{-3} NH_3, each period lasting about 5 hours on 14 and 15 November 2002 (see Figure 6). Readouts were obtained every 10 minutes. The used triplicates are indicated with black dots in Figure 6 (1 = high concentration (about 8 µg m^{-3}); 0 = transition period (between 0 and 8 µg m^{-3}); -1 = low concentration (about 0 µg m^{-3})).

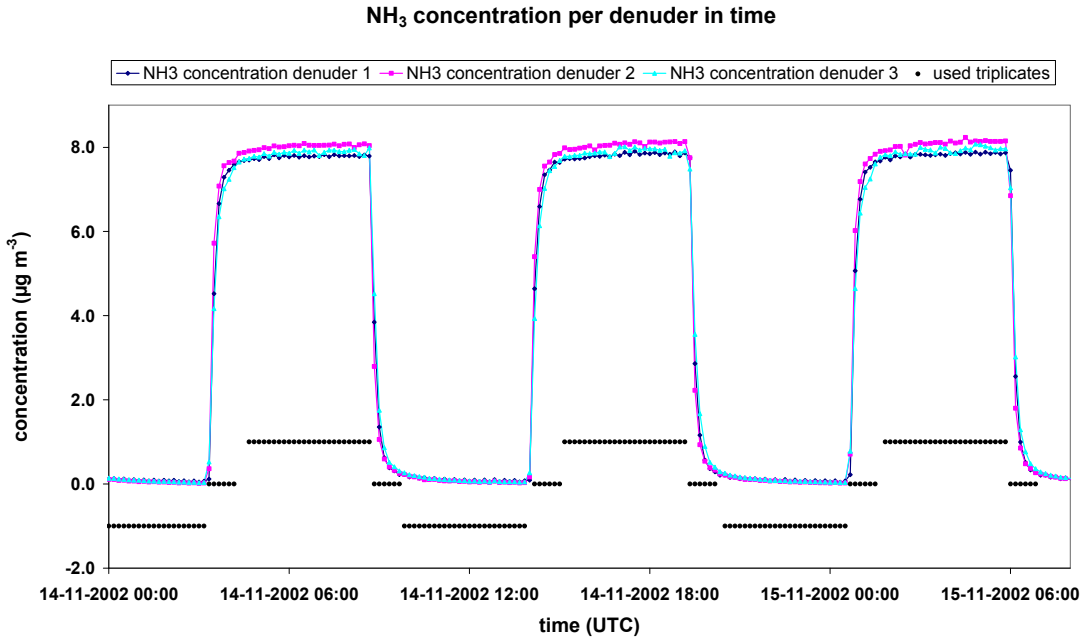

Figure 6. Laboratory concentration measurements for precision determination. The black diamonds represent the different situations during the concentration comparison test (1 = high concentration (about 8 µg m^{-3}); 0 = transition period (between 0 and 8 µg m^{-3}); -1 = low concentration (about 0 µg m^{-3}).

If we assume that the average of the three concentrations in Figure 6 is the 'real' concentration, we can distinguish two types of systematic errors. The first type is the difference in delay times between the

three individual denuders. Figure 7 shows the absolute difference between the individual denuders and the average of the three denuders (i.e. the 'real' concentration) versus the change of the average concentration in time. An increase in concentration in time will lead to a higher increase for denuder 2 than the average increase in concentration, i.e. denuder 2 is 'too fast'. Denuder 3 gives a lower increase than the average increase in concentration and can therefore be considered as 'too slow'.

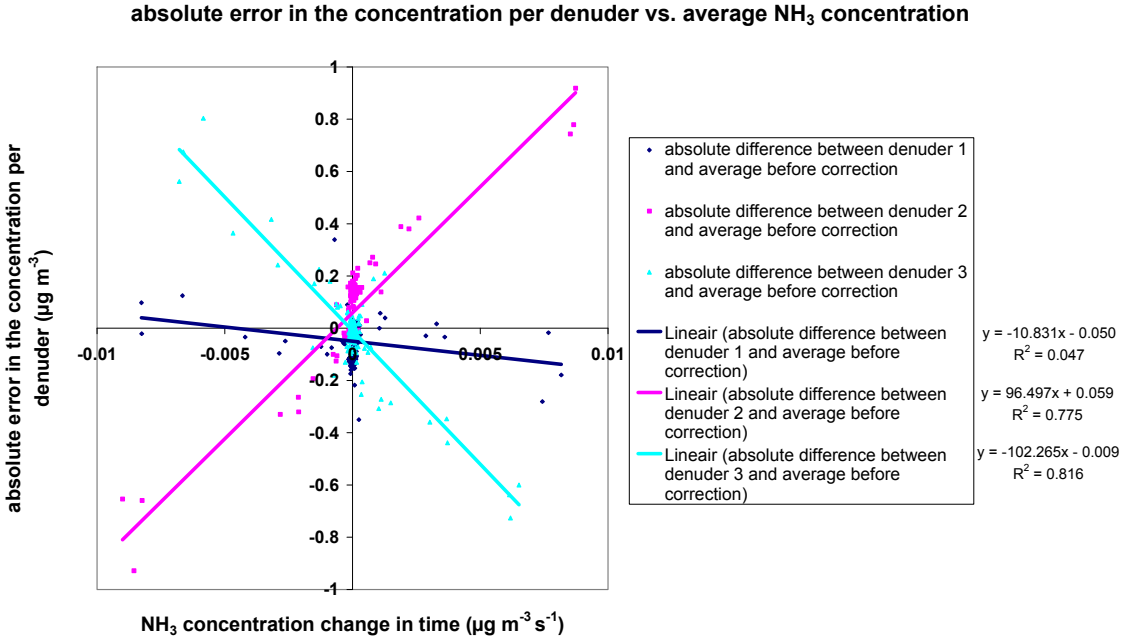

Figure 7. The absolute difference between each denuder and the average concentration versus the concentration change in time (µg m^{-3} s^{-1})

The second type of systematic error that was corrected is the regression of the measured concentrations per denuder (slope and offset) relative to the average concentration (Figure 8).

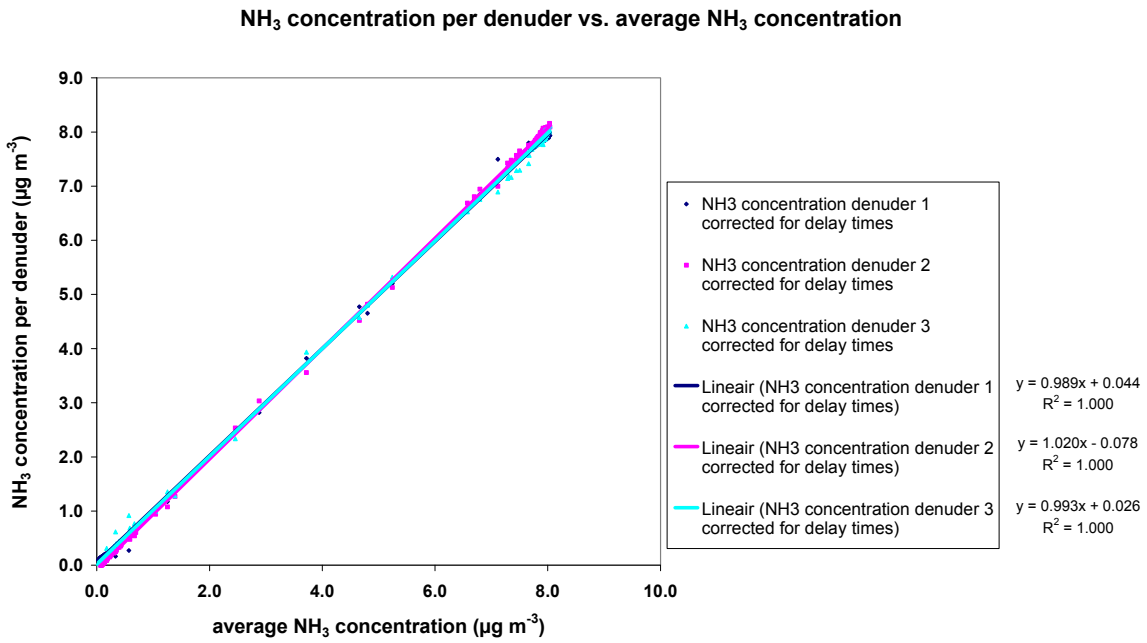

Figure 8. Linear regression through the measured concentrations per denuder relative to the average concentration after correction for the different delay times.

The figures below show the absolute difference between the measured concentrations per denuder and the average concentration before (Figure 9) and after (Figure 10) systematic error correction. The systematic error correction for the differences in delay times reduces the large peaks just after concentration change, while the systematic error correction for the linear regression reduces the differences between the individual denuders and the average.
The resulting absolute difference (between the measured concentration per denuder and the average concentration) after systematic error correction represents the random error (Figure 10). The figure shows that the random error is a little bit higher (and variable) in periods of quickly changing concentrations (transition periods), while it is rather low (and constant) in stationary conditions (around 0 and 8 µg m^{-3}).

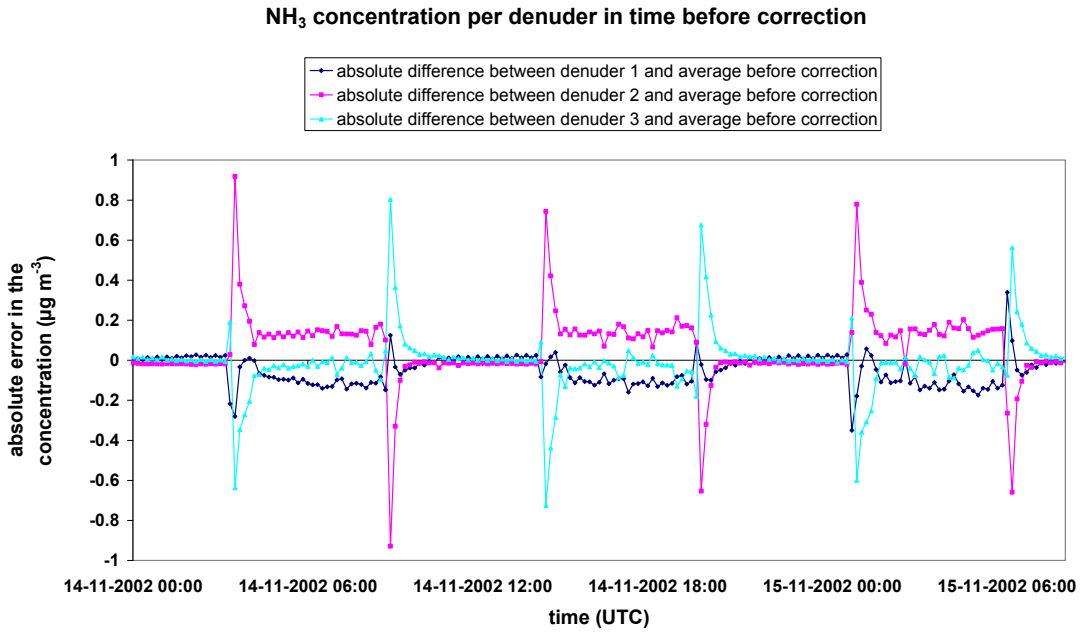

Figure 9. Absolute difference between the measured concentrations per denuder and the average concentration before systematic error correction.

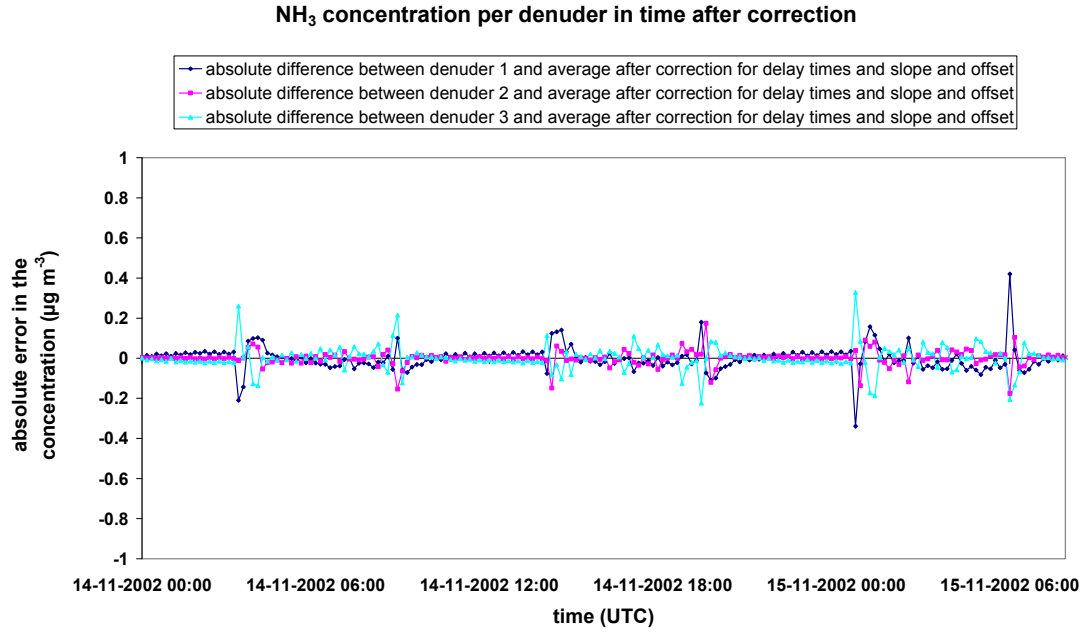

Figure 10. Absolute difference between the measured concentrations per denuder and the average concentration after systematic error correction.

In order to be able to compare the performance of the GRAHAM with the performance of AMANDA, every three subsequent results of each denuder were averaged in order to obtain one triplicate every 30 min. The results of the error analysis in the concentration measurements corrected for systematic errors are shown in Table 2. The table shows the random errors for two different averaging times, e.g. 10 and 30 minutes. We also distinguished three different regimes, e.g. 0 μg m^{-3}, between 0 and 8 μg m^{-3}, and 8 μg m^{-3}.

Table 2. Random errors in the concentration measurements corrected for systematic errors for two averaging times (10 and 30 minutes) and three periods (0 μg m^{-3}, 0-8 μg m^{-3} and 8 μg m^{-3})

	10-minute average		**30-minute average**	
	absolute random error	**Relative random error**	**Absolute random error**	**Relative random error**
average deviation of the mean concentration at 0 μg m^{-3}	0.012 μg m^{-3}	-	0.012 μg m^{-3}	-
number of triplicates	48	48	16	16
average deviation of the mean concentration between 0 and 8 μg m^{-3}	0.080 μg m^{-3}	2%	0.058 μg m^{-3}	1.45%
number of triplicates	36	36	12	12
average deviation of the mean concentration at 8 μg m^{-3}	0.027 μg m^{-3}	0.34%	0.018 μg m^{-3}	0.23%
number of triplicates	75	75	24	24

The random error in the 10-minute average data in this laboratory test is 0.027 μg m^{-3} at 8 μg m^{-3}, which corresponds to a relative random error of about 0.34%. The random error is even smaller at 0 μg m^{-3} (0.012 μg m^{-3}), but much higher in the transition periods, 0.080 μg m^{-3}. The relative random error in the transition periods (assuming an average concentration of 4 μg m^{-3}) is about 2% and can mainly be ascribed to the differences in delay times between the individual denuders. The random error in the 30-minute average data is 0.018 μg m^{-3} at 8 μg m^{-3}, which corresponds to a relative error of about 0.23%. The random error at 0 μg m^{-3} is 0.012 μg m^{-3} again and the random error in the transition period is 0.058 μg m^{-3} (or about 1.45%).

4.1.2 Field comparison

During a field comparison 'campaign' of 10 days in June 2004, a precision test was done with the attached PVC pipe (described in Chapter 3.2.2). Concentrations roughly varied between 4 and 50 μg m^{-3} during this period and all three denuders showed a similar pattern. To estimate random errors in the concentration measurements, data are corrected for systematic errors following the procedure described before. We only considered concentration measurements between 0 and 20 μg m^{-3} to have a homogeneous distribution of concentrations and to be sure that possible saturation effects were excluded. Before the systematic error correction, the average difference between each denuder and the average of the three denuders was 0.05 μg m^{-3} at an average concentration of 8.77 μg m^{-3}, so about 0.6 %. After systematic error correction, this difference is reduced to zero by definition.
Figure 11 shows the absolute difference between the individual denuders and the average of the three denuders versus the concentration change in time. This yields a systematic error correction due to differences in delay times between the individual denuders. Figure 12 shows the regression of the

measured concentrations per denuder (corrected for differences in delay times) relative to the average concentration. This is the second systematic error correction to correct for the slope and the offset.

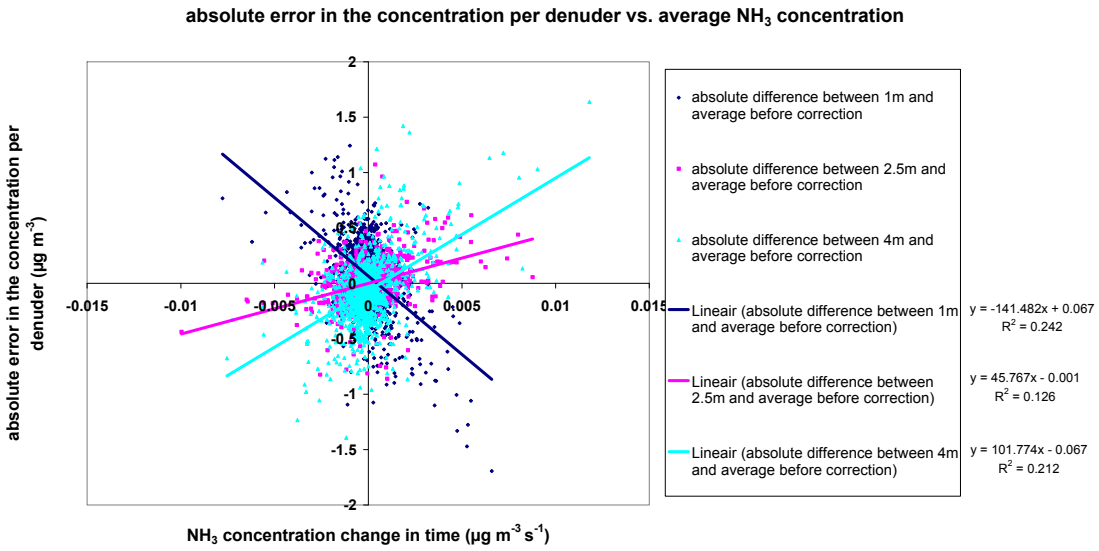

Figure 11. Absolute difference between each denuder and the average concentration versus the concentration change in time (µg m^{-3} s^{-1})

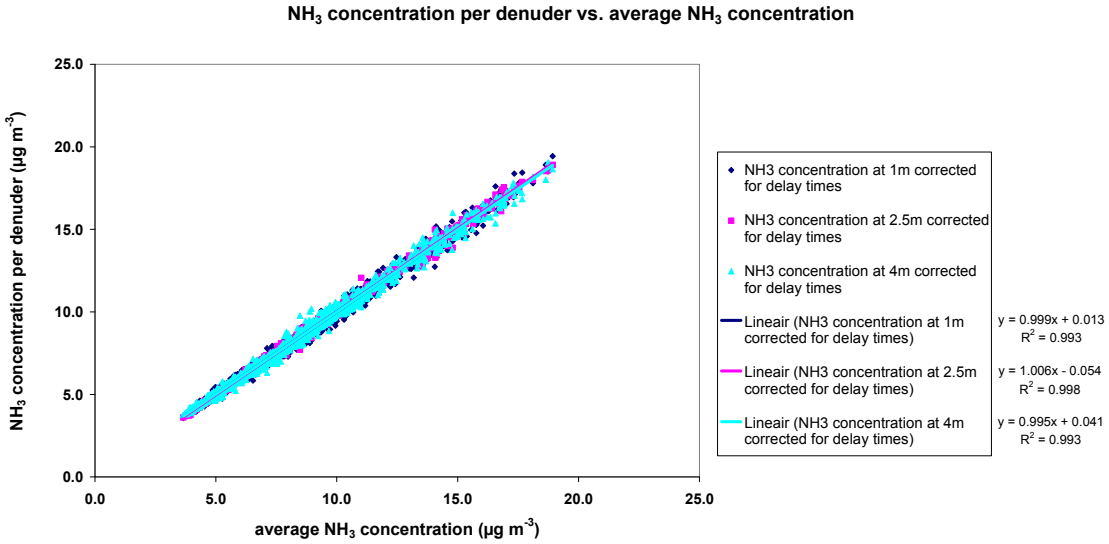

Figure 12. Linear regression through the measured concentrations per denuder relative to the average concentration after correction for the different delay times.

To compare the results from this field comparison with the results in the laboratory, the absolute between-instrument differences are calculated. Figure 13 shows the random error as a function of the average NH_3 concentration. The random error in the measurements increases with an increasing NH_3 concentration. The average slope of the random error is about 0.019 times (or 1.9% of) the

concentration. This means that the random error for an average concentration of about 8 µg m^{-3} is 0.16 µg m^{-3}.

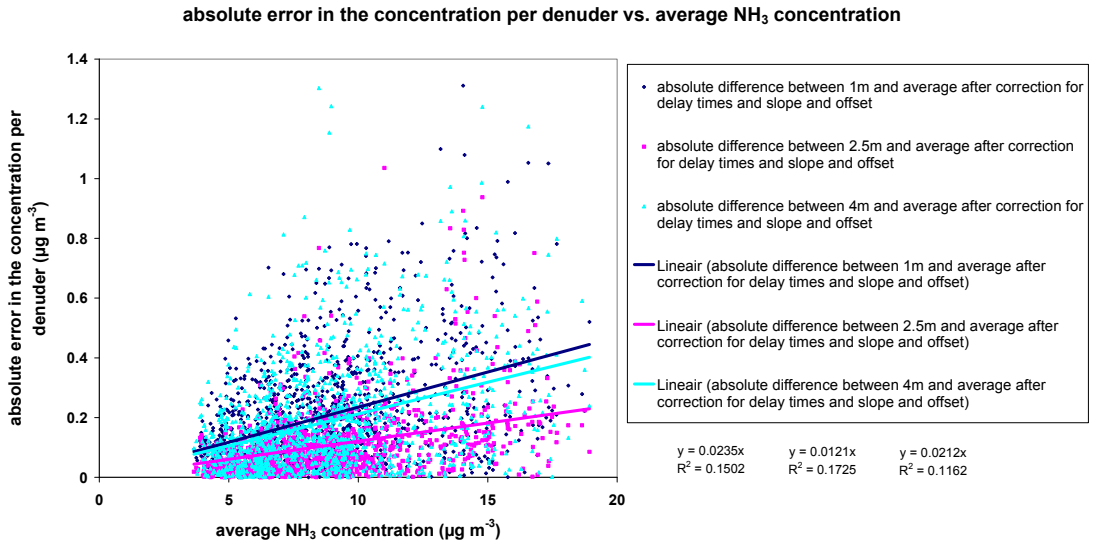

Figure 13. Random error as a function of the average NH_3 concentration for the three measurement heights.

We conclude that the precision of the instrument in the field (1.9%) is comparable to the precision of the instrument in the laboratory in transition periods (about 2%). Although the average concentration changes in the field are generally smaller than the concentration changes (8 µg m^{-3}) in the transition periods in the laboratory, weather influences such as substantial temperature and humidity changes are likely to affect the precision. In the presented results, a random error of 1.9% (based on the field comparison) is applied on the concentration measurements. The systematic error of 0.6% in the concentration measurements was corrected and is not present in the flux calculation. In Chapter 4.3, we will investigate how large the effect of this systematic error correction would be on our flux calculation (in the hypothetical case that we would not correct our concentration measurements for the known systematic errors).

4.2 Random error in the flux

For quantities that are a function of several parameters, a combined random error is calculated. The relative random error in our flux calculation, $F_\chi = -u_* \chi_*$ (Equation 6), is given as:

$$\frac{\delta F_\chi}{|F_\chi|} = \sqrt{\left(\frac{\delta u_*}{|u_*|}\right)^2 + \left(\frac{\delta \chi_*}{|\chi_*|}\right)^2} \qquad (16)$$

The random error in the friction velocity (δu_*) is calculated with the ECpack software developed by Wageningen University (Van Dijk et al., 2004; freely available at http://www.maq.wur.nl). Figure 14 shows that the relative random error in the friction velocity is about 4-5%. The relative random error in u_* is rather constant during the day, whereas relative random errors higher than 5% mainly occur during very stable and calm nighttime situations.

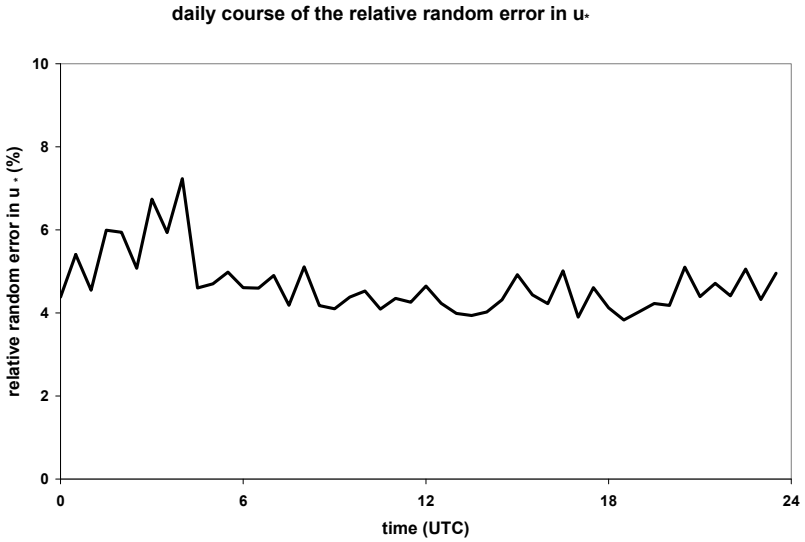

Figure 14. Daily cycle of relative random error in u_* for the entire data set.

The random error in χ_* is more difficult to determine. We start with rewriting Equation 10b into:

$$\chi_* = k\frac{\chi(z_2)-\chi(z_1)}{\ln\left(\frac{z_2}{z_1}\right)-\Psi_\chi\left(\frac{z_2}{L}\right)+\Psi_\chi\left(\frac{z_1}{L}\right)} \tag{17}$$

The relative random error in χ_* is described as:

$$\frac{\delta\chi_*}{|\chi_*|} = \sqrt{\left(\frac{\delta[\chi(z_2)-\chi(z_1)]}{|\chi(z_2)-\chi(z_1)|}\right)^2+\left(\frac{\delta f(z,\Psi)}{|f(z,\Psi)|}\right)^2} \tag{18}$$

where: $\delta[\chi(z_2)-\chi(z_1)] = \sqrt{(\delta\chi(z_2))^2+(\delta\chi(z_1))^2}$ represents the random error in the concentration difference (the numerator in Equation 17, shown as error bars in Figure 15 together with the daily cycle of the concentration difference), and $\delta f(z,\Psi)$ represents the random error in the stability corrected height (the denominator in Equation 17; abbreviated as $f(z,\Psi)$ in Equation 18). Assuming that the errors in the heights of the measurements (z_1 and z_2) are negligible, the error in the stability corrected height in Equation 18 is only determined by errors in the stability corrections. However, the errors in the stability corrections are difficult to determine as they are complex functions of the Obukhov length. In this study we assume a relative random error in the stability correction functions of 5% (Nieuwstadt, 1978; Holtslag and Van Ulden, 1983). Figure 16 shows the daily cycle of the relative random error in χ_* (Equation 18).

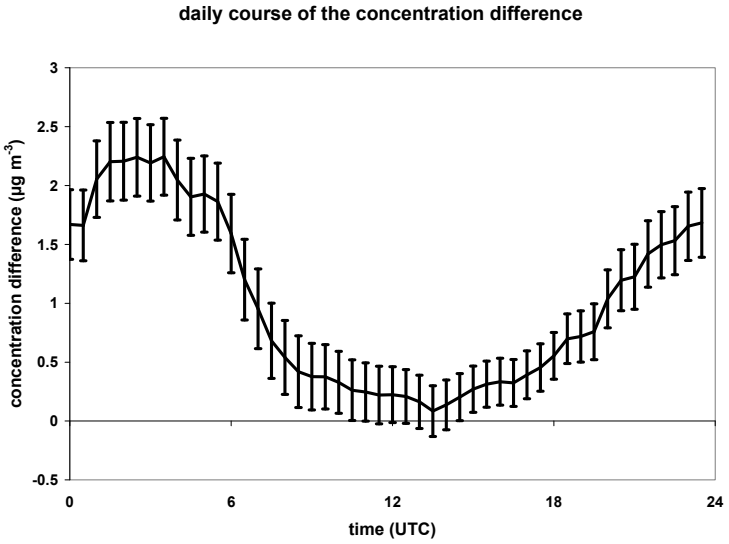

Figure 15. Daily cycle of the concentration difference for the entire data set.

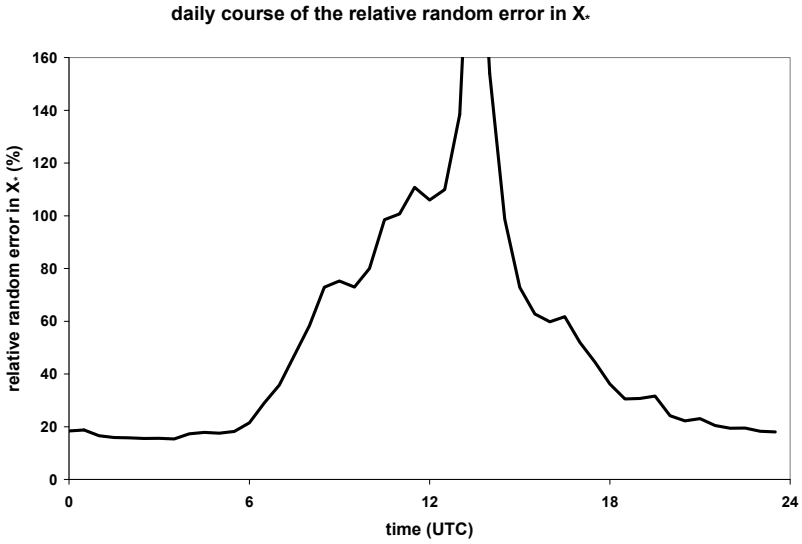

Figure 16. Average daily cycle of the relative random error in χ_* for the entire data set. (peak value is 255%)

The random error in the flux estimate is calculated by multiplying the relative error in the flux by the absolute value of the flux, according to:

$$\delta F_\chi = \left|F_\chi\right| \cdot \sqrt{\left(\frac{\delta u_*}{|u_*|}\right)^2 + \left(\frac{\delta \chi_*}{|\chi_*|}\right)^2} \qquad (19)$$

Figure 17 shows the random error in the flux estimate for the entire data set. The random error in the flux estimate is largest (about 0.06 µg m^{-2} s^{-1}) in the early morning and during daytime mainly due to

small concentration differences, whereas it is relatively small (about 0.01 µg m^{-2} s^{-1}) during night time, when concentration differences are relatively large. On average the random error in the flux estimate is about 0.03 µg m^{-2} s^{-1}.

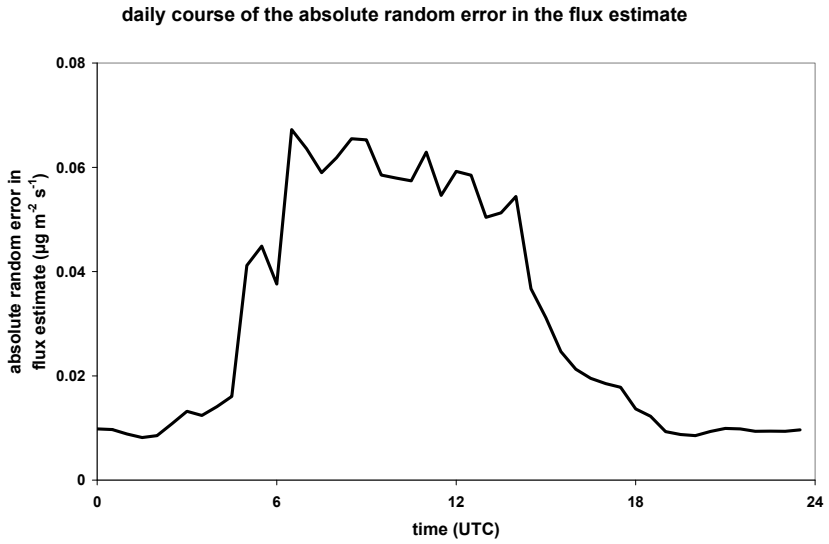

Figure 17. The daily cycle of random error in the flux estimate for the entire data set.

If we look at the relative random error in the flux measurement (Figure 18), i.e. the (absolute) random error in the flux divided by the flux, we see that the relative random error is rather small (in the order of about 20%) during night time, when the gradient is well defined, and becomes very large (over 100%) during daytime, when the concentration differences and consequently the fluxes approach zero.

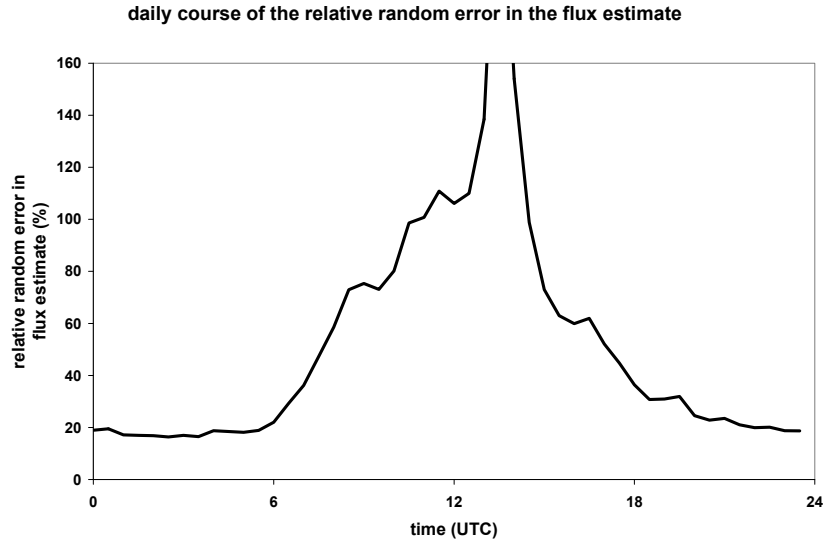

Figure 18. The daily cycle of relative random error in the flux estimate for the entire data set. (peak value is 255%)

Table 3 gives an overview of the observed ranges for the daily cycle of the different parameters in the flux calculation. It also shows the ranges for the absolute and relative random error in the different parameters in the flux calculation.

Table 3. Overview of ranges for the absolute and relative random error in the flux calculation parameters.

parameter	mean	Absolute random error	Relative random error
χ	10.0 μg m^{-3} (7.3 - 12.7)	0.19 μg m^{-3} (0.14 - 0.24)	1.9%
u_*	0.18 m s^{-1} (0.13 - 0.25)	0.008 m s^{-1} (0.006 - 0.011)	5% (4 - 7)
$\chi(z_2) - \chi(z_1)$	1.01 μg m^{-3} (0.08 - 2.24)	0.27 μg m^{-3} (0.20 - 0.34)	52% (15 - 255)
χ_*	0.41 μg m^{-3} (0.08 - 1.53)	0.16 μg m^{-3} (0.05 - 0.39)	52% (15 - 255)
F_χ	-0.07 μg m^{-2} s^{-1} (-0.02 - -0.24)	0.03 μg m^{-2} s^{-1} (0.01 - 0.07)	52% (15 - 255)

The relative random error in the flux calculation varies between 15% during night time and 255% during daytime. The average relative random error in the flux estimate is about 52% (the median value is 31%). Note that these large relative random errors are mainly caused by the (relatively small) random errors in the concentration measurements in combination with the small concentration differences.

4.3 Effects of systematic errors in concentration measurements on the flux

To investigate the effect of the systematic errors in the concentration measurements on the flux estimates (e.g. to see if systematic errors can lead to a different sign for the flux), we compared the flux measurements without correction for systematic errors with the flux measurements with corrections for systematic errors (like described in the previous Chapters). Figure 19 shows the daily cycle of the calculated systematic error in the flux estimate (flux without systematic error correction - flux with systematic error correction). The systematic error in the flux estimate is about 2 times smaller than the random error in the flux estimate (solid line compared to the dashed line). The systematic error in the flux estimate is largest in the morning (i.e. about 0.03 μg m^{-2} s^{-1}) mainly due to large concentration changes in time, while it is relatively small during night time (i.e. about 0.005 μg m^{-2} s^{-1}), when there might be large concentration changes, but there is minimum exchange.

Figure 20 shows the average daily cycle of the 'best' flux estimate (black solid line) with the random errors (error bars). The flux calculated without the systematic error corrections (black dashed line) does not significantly affect the pattern of the daily cycle of the flux and only seem to influence the size of the mean (annual) flux.

Several short comparison tests (of about 1 day) in 2004 indicate that the systematic error corrections obtained from the 10-day comparison period are representative for the whole period, although the slopes and the offsets might sometimes change sign (opposite systematic error correction) or are larger (larger systematic error correction) than the slopes and offsets used in this study. Since these short comparison tests only concern few measurements and a very limited concentration range, they are considered to be highly uncertain and inadequate for intermediate data correction. Therefore, we decided to use the systematic error corrections from the 10-day comparison period to correct all our data.

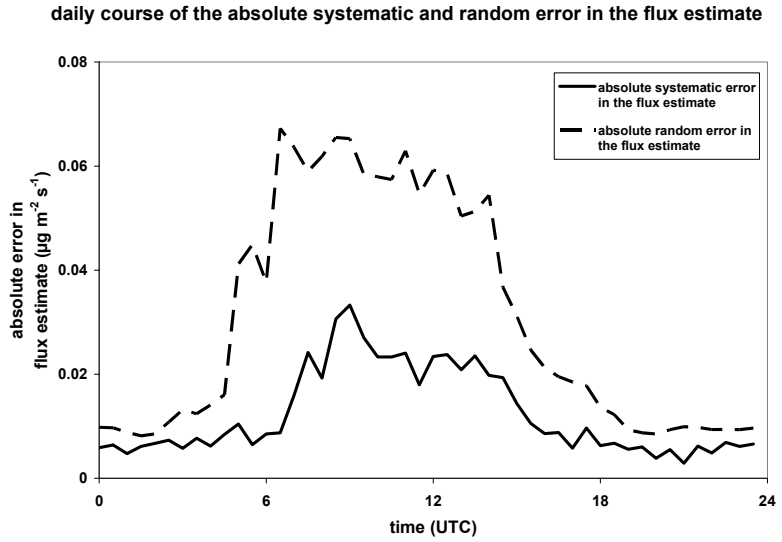

Figure 19. The daily cycle of the absolute systematic (solid line) and random (dashed line) error in the flux estimate for the entire data set.

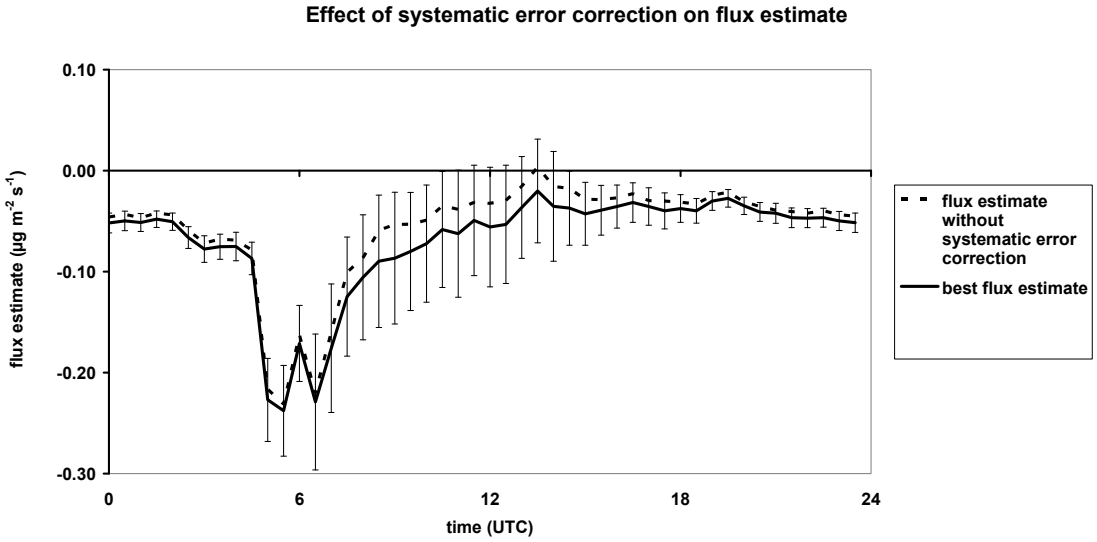

Figure 20. Average daily cycle of the flux estimate (solid black line) and the random errors (error bars) for the entire data set. The dashed line represents the flux estimate without systematic error corrections to show the sensitivity for systematic error corrections in the flux estimate.

4.4 Summary uncertainties and concluding remarks

4.4.1 Errors in the concentration

In a *laboratory comparison* test, a random error of 0.027 µg m^{-3} at 8 µg m^{-3} is found in the 10-minute average data after systematic error correction, which corresponds to a random error of about 0.34%. The random error at 0 µg m^{-3} is even smaller (i.e. 0.012 µg m^{-3}). On the other hand, the random error in the transition periods (between 0 and 8 and vice versa) is much higher, i.e. 0.080 µg m^{-3}, which corresponds to a ***random error*** of about 2% (assuming an average concentration of 4 µg m^{-3}).

In a *field comparison* test of 10 consecutive days, we obtained that the average ***systematic error*** in the concentration between the three denuders is about 0.6% at an average concentration of 8.7 µg m^{-3}. After systematic error correction, this systematic difference reduced to zero by definition. The random error in the concentration that remained after this systematic error correction was 0.17 µg m^{-3} at an average concentration of 8.7 µg m^{-3}, which corresponds to a ***random error*** of 1.9%.

So, the random error in a concentration measurement under field conditions (1.9%) is much larger than the random error in a concentration measurement under stable laboratory conditions (0.34%). This difference is mainly caused by a continuously changing concentration in the field, while in the laboratory the concentration was kept constant until it stabilized. The random error in the transition periods in the laboratory comparison of 2%, however, compares well with the random error found in the field comparison.

4.4.2 Errors in the flux

After correcting our concentration measurements for systematic errors, the flux can be calculated as described in Chapter 2.2. However, the random errors in the concentration measurements (1.9%) propagate in the flux calculations and result in an average ***random error*** in the calculated fluxes of 52% (median value is 31%). Large differences are observed between the random error in the flux calculation during nighttime (15%) and during daytime (255%). The large random errors during daytime are mainly caused by small concentration differences in combination with the random errors in the concentrations at the different heights. During nighttime, these concentration differences are considerably larger and consequently, the random error in the flux calculation is smaller.

If we would not correct our concentration measurements for systematic errors, an average ***systematic error*** in the flux calculation of 18% would be made. However, because we assume that the systematic error corrections are justified and correct, there is no systematic error present in our final flux calculation. However, if the systematic error correction in the concentration measurements is applied unjustified, the error that we make in the flux calculation as a consequence of the systematic error correction is relatively small (18%) compared to the random error in the flux calculation (52%) on an hourly basis.

5 Overview of NH_3 flux measurements and derived variables

In this section an overview of the available concentration measurements, flux measurements and derived variables is given. For practical reasons, hourly values are derived from the half-hourly measurements in this overview. The total number of hourly measurements (for which two half-hourly measurements were available) in 2004, 2005 and 2006 is 8593, which is about 33% of this three year period. In order to select the reliable ammonia profiles, a selection from these 8593 hours was made based on several quality criteria. The reasons for applying the criteria for data acceptance were discussed in the previous chapters and will only be mentioned briefly here. The percentage of rejected data is given per criteria in parenthesis.

- Concentration larger than detection limit, i.e. 0.02 µg m^{-3}; here a lower limit of 1 µg m^{-3} was used (1.0%)
- Stationary conditions, i.e. concentration change < 20 µg m^{-3} hr^{-1} and flux < 0.5 µg m^{-2} s^{-1} (5.2% respectively 2.4%)
- No extremely stable or unstable meteorological conditions, i.e. $|L| > 5$ (15.0%)
- Profile determined by its direct environment, e.g. no external influence of farms or neighbouring fields, i.e. CNF > 0.75 (32.3%)

Some of the criteria have an overlap with one or more of the other criteria, e.g. the criteria for the CNF and L (as L is included in the formulation for CNF). The total reduction of the number of hourly measurements as a consequence of the criteria is 41.9%. This means that from the available 8593 hours, 4994 are used for further analysis.

Table 4 gives an overview of the percentage and number of hourly measurements available per month after application of the quality criteria in the years 2004, 2005 and 2006. In the months November, December, January, February and March relatively few data are available due to (yearly) maintenance of the instrument and cold weather conditions during which the instrument is switched off to prevent it from freezing. Exception is the warm winter of 2006/2007. In the summer of 2006 extremely high temperatures (>35 degrees Celsius) and a technical failure have reduced the data coverage.

Table 4. Availability of flux measurements per month accounting for quality criteria (between brackets availability without quality criteria). Months with a data coverage of more than 30% are marked in yellow.

	2004		2005		2006	
month	%	hours	%	hours	%	hours
January	0%(0%)	0(0)	0%(0%)	1(2)	0%(0%)	0(0)
February	0%(0%)	0(0)	10%(21%)	64(141)	0%(0%)	0(0)
March	0%(0%)	0(0)	24%(36%)	177(265)	0%(0%)	0(0)
April	0%(0%)	0(0)	33%(62%)	239(443)	31%(58%)	223(416)
May	0%(0%)	0(0)	26%(46%)	196(340)	60%(84%)	446(623)
June	14%(27%)	99(191)	0%(0%)	0(0)	19%(37%)	135(268)
July	34%(54%)	250(404)	16%(24%)	119(175)	16%(32%)	117(236)
August	33%(68%)	243(509)	35%(63%)	259(469)	9%(13%)	70(97)
September	14%(20%)	99(141)	33%(63%)	239(451)	19%(51%)	137(364)
October	46%(74%)	342(547)	37%(76%)	275(564)	51%(82%)	383(609)
November	1%(3%)	6(23)	20%(28%)	142(201)	36%(67%)	259(481)
December	0%(0%)	0(0)	0%(0%)	0(0)	64%(85%)	474(633)
yearly average	12%(21%)	1039(1815)	20%(35%)	1711(3051)	26%(43%)	2244(3727)

The figures below give an overview of the measured concentrations and fluxes and the derived deposition velocity and surface resistance in the years 2004, 2005 and 2006. The colored lines are the different years (2004 = cyan, diamonds; 2005 = magenta, squares; 2006 = purple, triangles), the black line (closed circles) represents the average daily cycle of all measurement data (or the sum, for the frequency distributions) and the black vertical lines give the 25-percentile and the 75-percentile values of all measurement data.
The figures give a picture of the measured data in each year and do not have to be representative for a whole year. Based on the measurements only, it is not possible to draw any conclusions from the differences between years. As such the data can only be used to study processes underlying the surface/atmosphere exchange of ammonia. Despite this restriction, we give an indicative overview of the results per year and try to explain the differences.

In Figure 21, the average daily cycle (average of all measurement data at a single time) of the concentration is shown. The concentration for each year is highest in the early morning. In 2004 and 2005 the average concentrations are a little higher than in 2006, which is possibly caused by the large content of winter data in 2006.
The average concentrations are 7.5, 8.4 en 6.1 µg m^{-3} in 2004, 2005 en 2006. The average concentration for all measurement data is 7.2 µg m^{-3}. The yearly spread of the data is shown by the error bars, which represent the 25-percentile and 75-percentile values (in between 50% of the data are present). The figure shows that 50% of the concentration measurements lie between 3.4 and 8.8 µg m^{-3}.

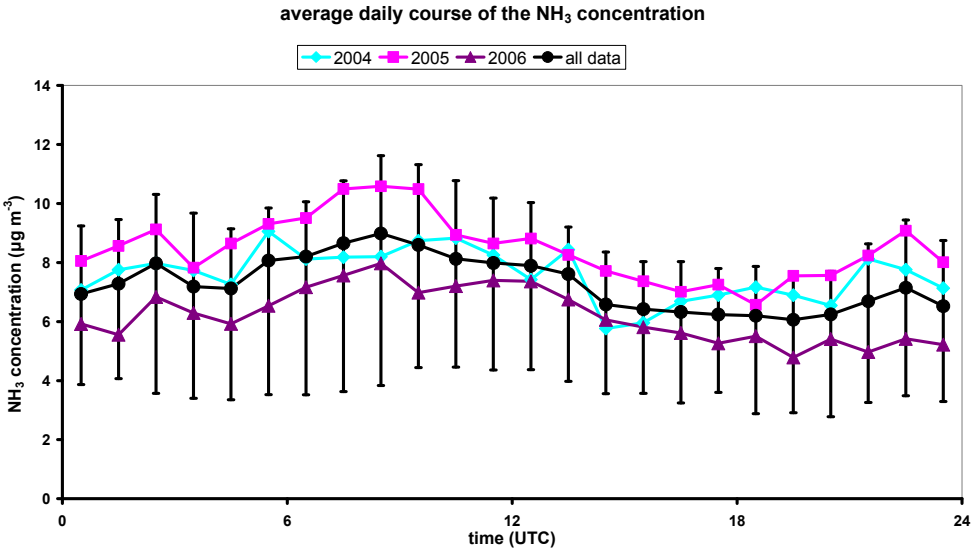

Figure 21. Average daily cycle of the ammonia concentration.

In Figure 22 the frequency distributions of the concentrations in the years 2004, 2005 and 2006 are shown. The figure clearly shows that 2006 has a higher measurement density, especially in the low concentration range. The measurements in 2006 are mainly done in the autumn and winter periods in which the concentrations are relatively low. In contrast, the frequency distributions in the years 2004 and 2005 are mainly caused by measurements in summer and autumn. This is one of the reasons for the difference in average concentration between these years.

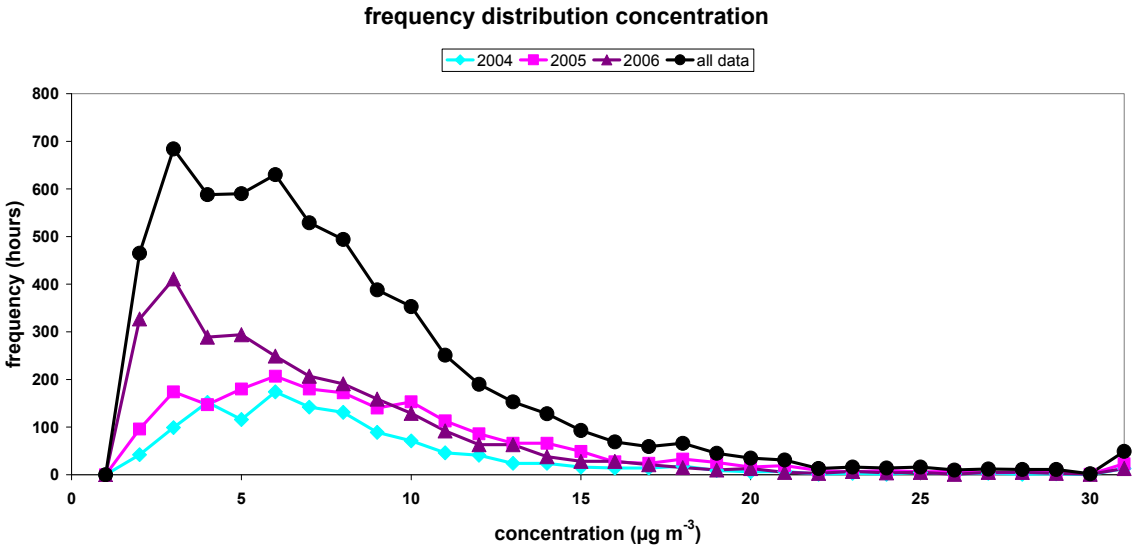

Figure 22. Frequency distribution of the concentration.

In Figure 23 the average daily cycle of the ammonia flux is shown. It is remarkable that the average daily cycle of the flux differs so strongly from year to year. Like the average daily cycle of the concentration, the daily cycle of the flux is strongly influenced by the season and the weather conditions during the measurements. The spread of the data is shown by the error bars again, which represent the 25-percentile and 75-percentile values (in between 50% of the data are present). These error bars show that there are mainly deposition (negative) fluxes. The average fluxes are -0.018, -0.043 and -0.083 µg m^{-2} s^{-1} in 2004, 2005 and 2006. The average flux of all data is -0.056 µg m^{-2} s^{-1}. The spread of all data is 0.061 µg m^{-2} s^{-1}, which means that 50% of all data are between -0.082 and -0.020 µg m^{-2} s^{-1}. Emission fluxes were particularly present in 2004 as showed in Figure 23.

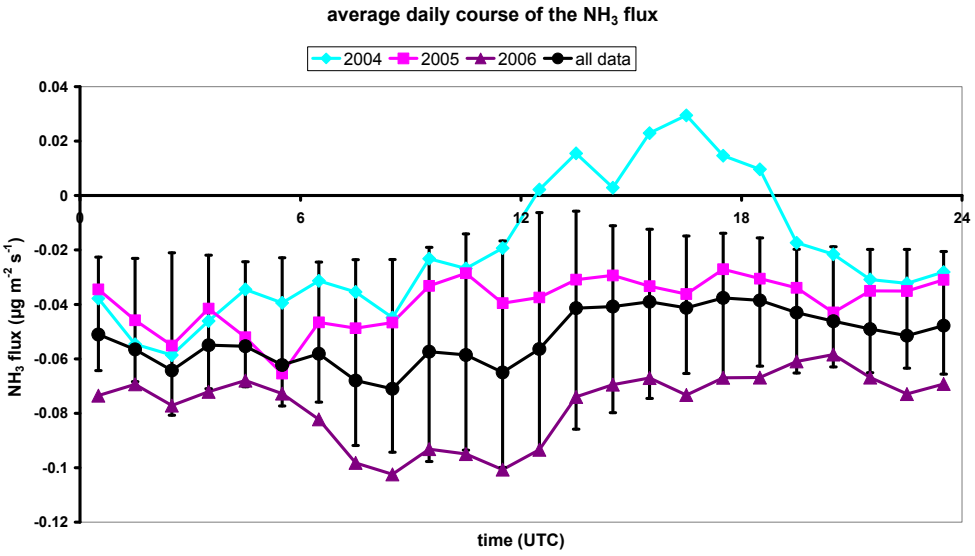

Figure 23. Average daily cycle of the ammonia flux, positive = emission and negative = deposition.

The frequency distributions of the deposition flux in Figure 24 show that in all years the (negative) deposition fluxes dominate, but also that there is a substantial number of emission cases in each year.

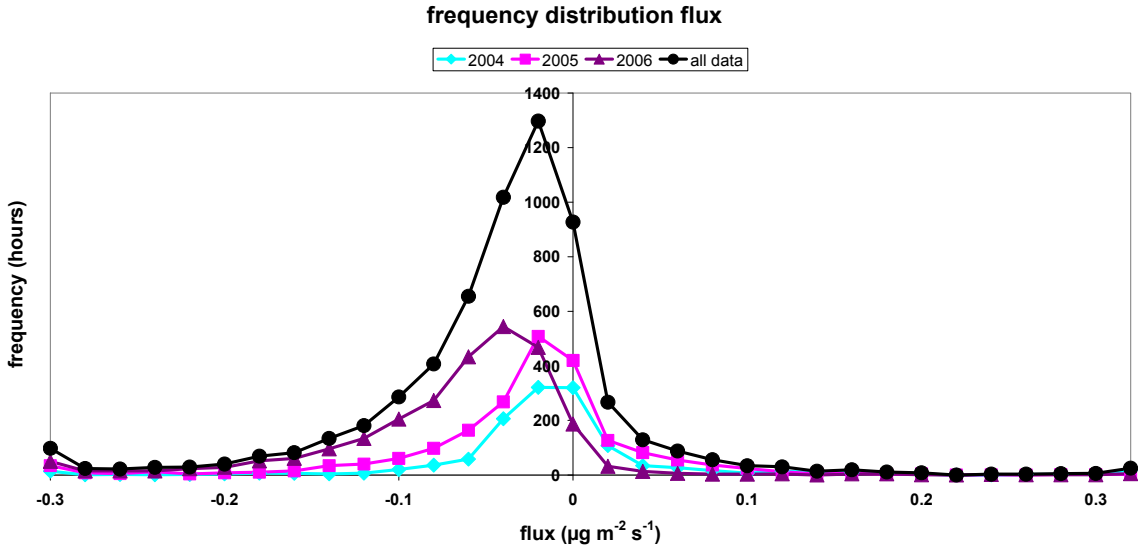

Figure 24. Frequency distribution of the ammonia flux, positive = emission and negative = deposition.

In Figure 25, we tried to explain the differences between the different years that we observed in Figure 21 till Figure 24 with the average daily cycles of surface temperature (upper panel), global radiation (middle panel) and relative humidity (lower panel). Note that only the hours for which NH_3 flux (and/or concentration) measurements were available, are considered here. Figure 25 nicely illustrates why it is difficult to mutually compare the different years.
The upper panel clearly shows that the surface temperature during the NH_3 flux measurements in 2004 was about 2 degrees Celsius higher compared to the other two years. A higher temperature will lead to higher internal plant concentrations (compensation points) and consequently less deposition or even emission.
The middle panel shows that in 2006 the measurements were carried out during less sunny conditions than in 2004 and 2005. Radiation is a driving force in the photosynthetic activity of plants and therefore the stomatal opening. Less radiation will lead to less stomatal opening and likely also to less emission events.
The lower panel shows the average daily cycle of the relative humidity in the measurement period. The relative humidity was relatively high during daytime in 2006 compared to 2004 and 2005 (about 5% higher). A high relative humidity will lead to a relatively wet external leaf surface and consequently a preference for deposition of ammonia towards the leaf surface.

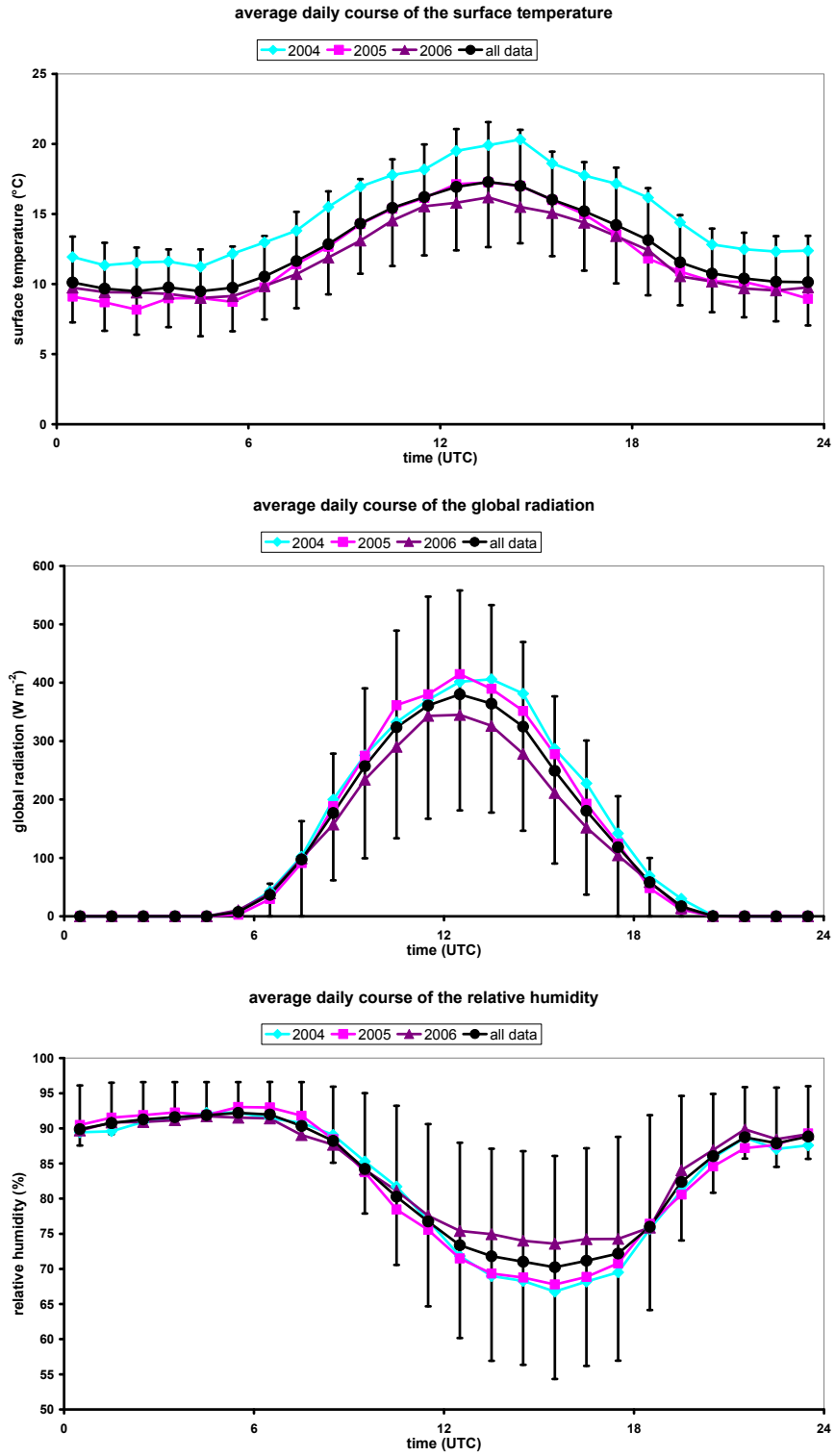

Figure 25. Average daily cycle of the surface temperature (upper panel), global radiation (middle panel) and relative humidity (lower panel) during the NH_3 flux measurement and flux estimate period.

In the atmospheric transport model OPS that is used at RIVM, the ammonia concentration is calculated as the product of a deposition velocity and the ambient concentration. The deposition velocity is an important quantity to characterize the deposition process. The deposition velocity at a certain height is defined as the quotient of the flux and the concentration at that height:

$$v_{d,1m} = -\frac{F_{NH3}}{C_{NH3,1m}} \qquad (20)$$

The relative random error in the deposition velocity is dominated by the relative random error in the flux, because the relative error in the concentration (about 1.9%) is very small compared to the relatively error in the flux (more than 20%) as already shown in Figure 18.

Figure 26 shows the average daily cycle of the deposition velocity at 1 meter height. A negative deposition velocity means emission of ammonia. The figure shows that especially in 2004 reduced deposition or even emission occurred between 6 and 18 UTC, while 2006 hardly shows any daily cycle and much higher deposition velocities. The negative deposition velocities in 2004 can be explained by the higher temperature in that year. These higher temperatures lead to higher surface concentrations and therefore reduced deposition or emission. The higher (positive) deposition velocities in 2006 can be explained by the lower global radiation and higher relative humidity in that year. Lower global radiation reduces emission from the stomata; higher relative humidity enhances surface wetness, which is favorable for deposition (as ammonia dissolves well in water layers on the leaf surface). On average, the deposition velocity at 1m for 2004, 2005 and 2006 amounts to 0.005, 0.007 and 0.017 m s^{-1} respectively. For all measurement data the average deposition velocity is about 0.011 m s^{-1}. The spread of the data (shown by the error bars, which represent the 25-percentile and 75-percentile values) is 0.013 m s^{-1}, which means that 50% of the data are within the range between 0.004 and 0.017 m s^{-1} (deposition). The frequency distributions of the deposition velocity in Figure 27 confirm the picture that is outlined above.

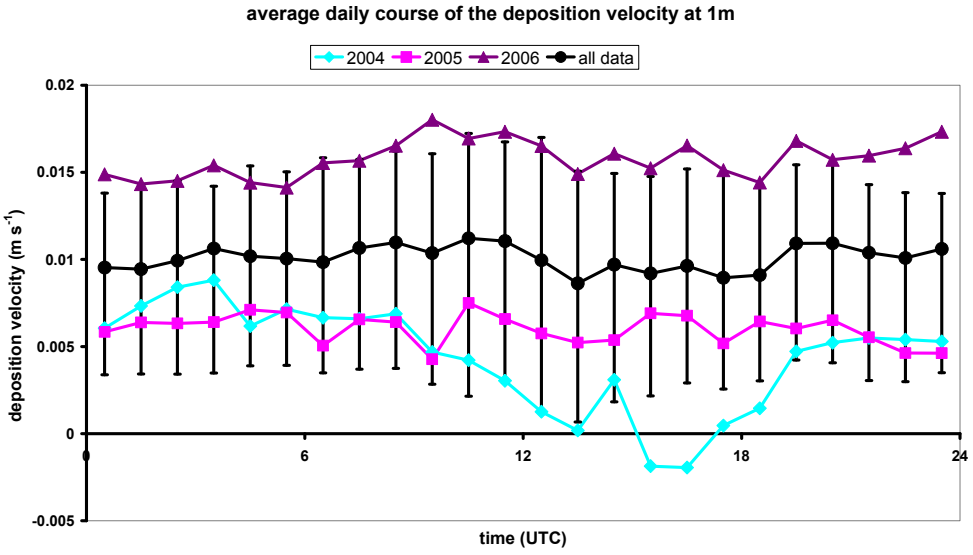

Figure 26. Average daily cycle of the deposition velocity at 1m height, positive = deposition and negative = emission.

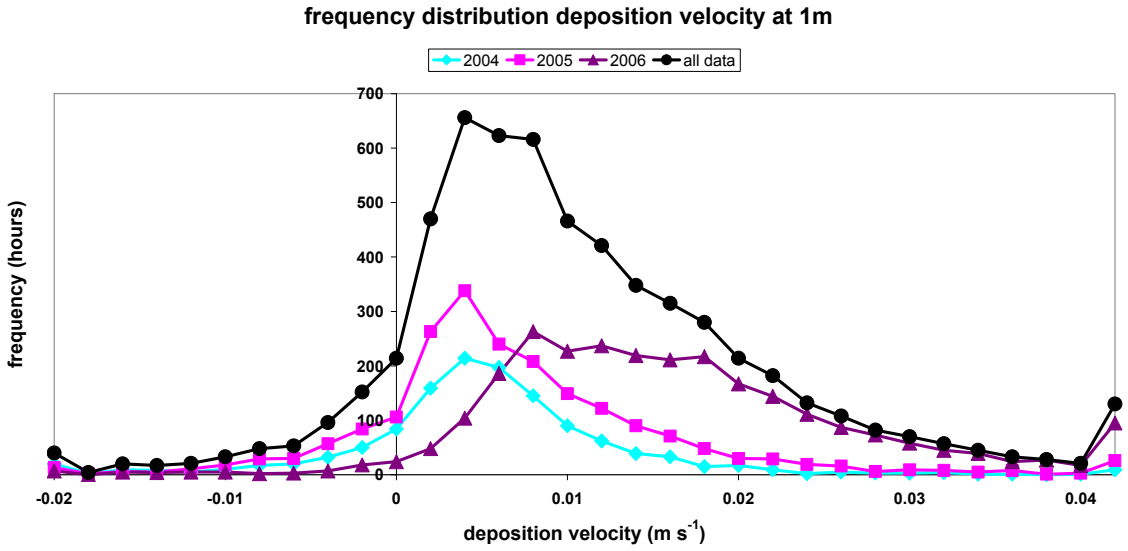

Figure 27. Frequency distribution of the deposition velocity at 1m, positive = deposition and negative = emission.

The different deposition pathways, along which ammonia deposits, are represented with resistances. The most simple form of this resistance approach assumes that the concentration at the surface is zero or in other words, the potential difference (concentration in the air minus the concentration at the surface (= 0)) is only determined by the concentration of ammonia in the air. The actual ammonia flux towards the surface is determined by the air concentration and the total resistance that ammonia experiences on its way towards the surface. This total resistance consists of an atmospheric resistance ($R_{a,1m}$), a quasi-laminar leaf boundary layer resistance ($R_{b,NH3}$) and a surface resistance (R_c). For ammonia, the surface resistance (R_c) is especially important because this resistance determines how much ammonia deposits on the surface. The atmospheric and the leaf boundary layer resistance are rather well known from meteorological measurements and therefore the surface resistance is calculated from the concentration and the flux estimate according to:

$$R_c = -\frac{C_{NH3,1m}}{F_{NH3}} - R_{a,1m} - R_{b,NH3} \qquad (21)$$

However, as can be seen in Figure 23 and Figure 24, the assumption that the surface concentration is zero is not always correct since emission fluxes are regularly observed. These emission fluxes only occur if the concentration at the surface is higher than the concentration in the air. In principle, this resistance approach is too simple for ammonia and a more complex compensation point model is needed to model the bi-directional fluxes. However, many atmospheric transport models (like the OPS model at RIVM) still use this simple approach because of model limitations. To provide these models with input, the surface resistance, R_c, is derived from the flux measurements, even though this gives considerable problems in the derivation and interpretation of these resistances. Therefore, the surface resistance is a very uncertain factor in atmospheric transport models.

Besides the conceptual shortcomings, the derived R_c from the measurements also contains the uncertainties from the flux and concentration measurements as well as the uncertainties in $R_{a,1m}$ and $R_{b,NH3}$. As we have seen in many of the previous figures, the ammonia flux is often close to zero or even positive (emission). In the surface resistance calculations from Equation 21, infinite or negative resistances are obtained in these situations. This generates an enormous spread in the measured R_c-values and makes it very complex to calculate a simple arithmetical average value. Therefore, a

reciprocal averaging (or harmonic averaging) is used. The idea is that the arithmetical averaging may be applied to the reciprocal of the resistance i.e. the conductance. An extremely high resistance leads to a very small conductance and this very small conductance has little influence on the average.
Figure 28 and Figure 29 show the average daily cycle and the frequency distribution of $1/R_c$ for the different years respectively. By using this harmonic averaging method we obtain an average $1/R_c$ value of 0.009 m s^{-1} in 2004 (~ $R_{c,har}$ of 106 s m^{-1}), 0.006 m s^{-1} (~ $R_{c,har}$ of 178 s m^{-1}) in 2005 and 0.007 m s^{-1} (~ $R_{c,har}$ of 148 s m^{-1}) in 2006. The average $1/R_c$ of all data is 0.007 (~ $R_{c,har}$ of 144 s m^{-1}). However, the spread in $1/R_c$ is very large (the difference between the 25% and 75% percentile values is 0.030 m s^{-1}).
The frequency distribution of $1/R_c$ shows a clear peak around 0.005 (R_c ~ 200) in 2004 and 2005. In 2006 this peak is less pronounced around 0.015 (R_c ~ 70). The observed range of $1/R_c$ values of all data is between -0.01 and 0.05. Consequently, R_c values correspond to two ranges of values, i.e. -100 to -∞ and 20 to ∞. The negative $1/R_c$ (and R_c) values occur in emission periods.

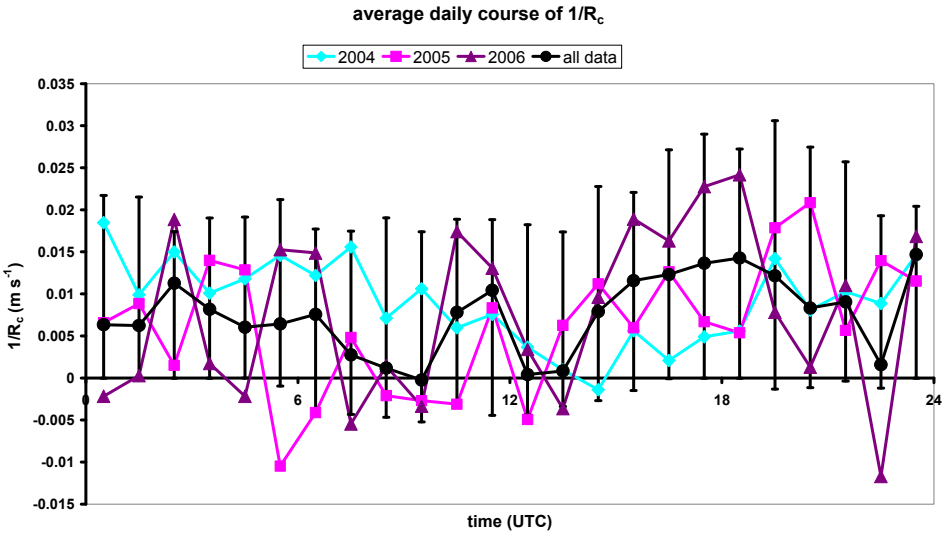

Figure 28. Average daily cycle of the reciprocal surface resistance.

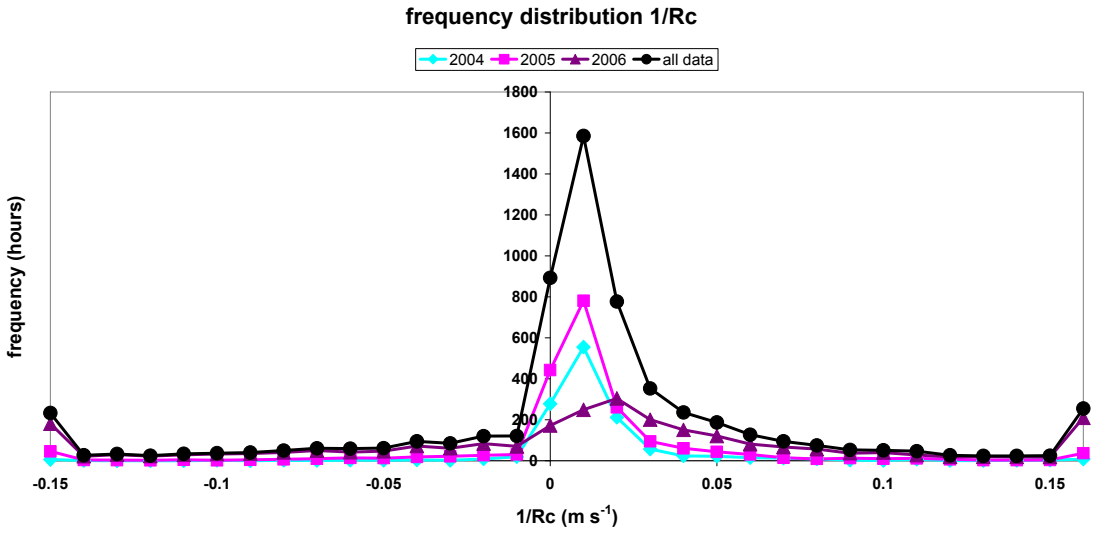

Figure 29. Frequency distribution of the reciprocal of the surface resistance.

Another way to calculate R_c is by using the average daily cycle of the concentration and the flux estimate and the average daily cycle of the median $R_{a,1m}$ and $R_{b,NH3}$ values in Equation 21. Figure 30 shows the derived average daily cycle of R_c. The error bars are calculated from the 25- and 75-percentile values of the flux, concentration, $R_{a,1m}$ and $R_{b,NH3}$. The differences between the three years are very large (as expected), however, the average R_c value of 67 s m^{-1} for all data and its reciprocal value of 0.015 m s^{-1} are well within the same range of R_c and $1/R_c$ values obtained with the harmonic averaging method, i.e. 20 to ∞ and -0.01 to 0.05 respectively.

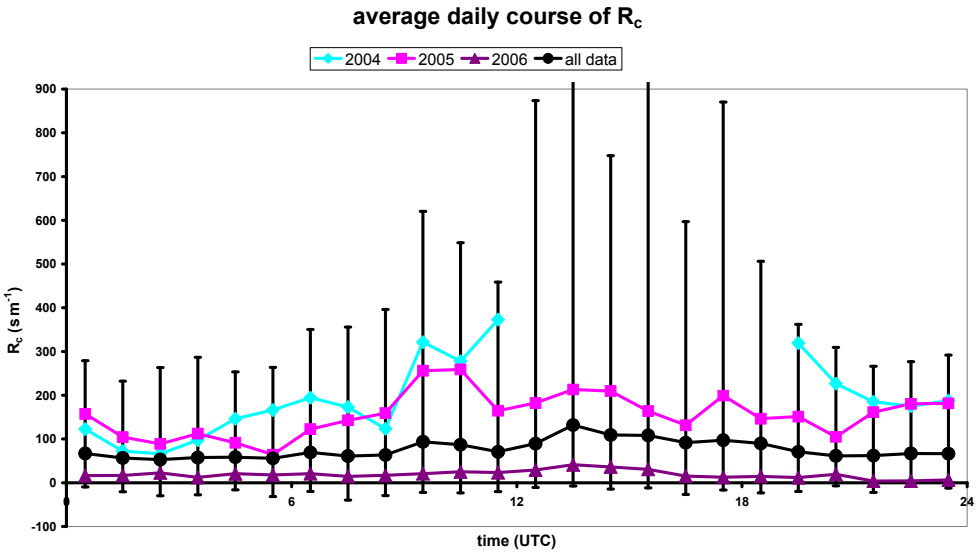

Figure 30. Average daily cycle of the surface resistance.

6 Discussion and Conclusion

In this report, the NH_3 flux measurements above grassland at the Haarweg in Wageningen is described. We furthermore describe the applied data selection procedure, the measurement site and the instrumentation. We also give an analysis of the random and systematic errors in the concentration measurements and consequently the flux measurements. After correction for the known systematic errors in the concentration measurements, the relative random error in the concentration is 1.9%. The relative random error in the NH_3 flux measurements is on average about 50%. We showed that the relative random error in the NH_3 flux measurements is much smaller during night time (about 20%) than during daytime (more than 100%). Reason for this is that the concentration differences are generally large during night time. The random error in the concentration is then relatively small compared to the concentration difference that determines the final flux. During daytime the concentration difference is generally much smaller, as a result of which the random error in the concentration is relatively large.
The surface resistance, R_c, is essential in model parameterisations that describe the deposition process of ammonia to the surface. The model parameterisations for R_c are derived from the R_c values that are deduced from the flux and concentration measurements as well as the aerodynamic resistances. The random error in the R_c parameterisation therefore includes all the random errors of all these variables, of which the random error in the flux measurement is largest most of the time.

Characteristic (harmonic) averaged values for R_c are shown in Table 5 for certain periods to further specify the surface resistance, R_c, to show the day/night and the seasonal dependency. To place these values in perspective, we also included deposition measurements from previous measurement campaigns by ECN over fertilized grassland in Schagerbrug and Zegveld. The table shows the harmonic averaged values for R_c for the deposition measurements in Wageningen (non-fertilized grassland), Schagerbrug (fertilized grassland, Mosquera et al., 2001) and Zegveld (fertilized grassland, Plantaz, 1998) for three different periods and for day versus night.
For Zegveld no raw data were available and therefore the calculated R_c values of Plantaz (1998) were given. The columns display the different periods; November – January is the winter period in which manure application is prohibited, February – April is the period in which manure is applied, and May – October is the growing (and grazing) season. The rows represent the different locations (Wageningen, Schagerbrug and Zegveld), day/night differences and the selection for which the harmonic average is valid (only deposition fluxes ($F < 0$), only emission fluxes ($F > 0$), or all data). The table also presents the percentage of deposition fluxes per period.

Table 5. Harmonic averaged R_c values for three flux measurement campaigns over Dutch grassland: Wageningen (2004-2006), Schagerbrug (1998-2000) and Zegveld(1992-1994).

		November-January	February-April	May-October	all data
R_c (night) Wageningen Non-fertilized grassland	F < 0	51	53	91	69
	F > 0	-446	-255	-412	-347
	all data	**52**	**74**	**102**	**78**
	% deposition flux	97%	77%	91%	91%
R_c (day) Wageningen Non-fertilized grassland	F < 0	96	30	62	57
	F > 0	-513	-220	-276	-264
	all data	**103**	**50**	**90**	**81**
	% deposition flux	94%	65%	75%	76%
R_c (night) Schagerbrug Fertilized grassland	F < 0	76	109	154	123
	F > 0	-144	-165	-141	-146
	all data	**-2320**	**262**	**-978**	**193**
	% deposition flux	32%	65%	45%	49%
R_c (day) Schagerbrug Fertilized grassland	F < 0	232	131	136	139
	F > 0	-117	-157	-137	-138
	all data	**-261**	**-4014**	**-1687**	**-1221**
	% deposition flux	37%	44%	46%	45%
R_c (night) Zegveld Fertilized grassland	F < 0	35	100	80	
R_c (day) Zegveld Fertilized grassland	F < 0	65	105	95	

In deposition cases (F < 0), the average R_c values are relatively low. Non-fertilized grassland has a smaller R_c value than fertilized grassland as well during daytime as during night time. In emission cases (F > 0), negative R_c values were found for fertilized grassland as well as for non-fertilized grassland. The values for fertilized grassland are smaller (less negative), which means that the emissions from fertilized grassland are larger, as expected. If both emission and deposition fluxes are considered, the harmonic averaged R_c values become larger. For non-fertilized grassland, a harmonic averaged R_c value of about 80 s m^{-1} is found for nighttime as well as for daytime. For fertilized grassland mainly negative R_c values are found, which means that as well in the daytime as at night emissions occur. If only the deposition cases (F < 0) are considered, high (positive) R_c values are found, which means that deposition is strongly suppressed.
In general, no clear seasonal dependency in the R_c values seems to exist as the fluctuation in the harmonic averaged R_c values over the seasons is very large.

Cuticular (or external leaf surface) resistance, R_w
The uptake of ammonia at the surface mainly occurs through the leaf stomata, by the cuticles (or external leaf surface) and by the soil. Each of these deposition pathways can be represented by a

resistance. By measuring the evapotranspiration of water by the vegetation a value for the stomatal resistance, R_s, is obtained. The stomatal resistance is rather well known (Wesely, 1989; Baldocchi et al., 1987). The uncertainties in the cuticular resistance is however very large. Many studies (Erisman et al., 1994; Duyzer et al., 1994; Jakobsen et al., 1997; Nemitz et al., 2004) have shown the dependency of R_w on relative humidity (RH). Reason for this is that the leaf surface is getting moister or wetter at higher humidity and that ammonia as a result dissolves easier, which reduces the resistance to uptake. The cuticular resistance, R_w, is often derived from the nocturnal surface resistance, R_c(at night), when stomata are closed and the stomatal resistance is assumed to be infinitely large. Theoretically, this nocturnal surface resistance consists of both the cuticular resistance, R_w, and the soil resistance, R_{soil}. However, especially for dense grassland vegetation, the soil pathway is cut off.
Figure 31 shows the dependency of R_w on relative humidity for fifteen different field studies over different vegetations in different pollution climates. In this study only deposition fluxes are considered.

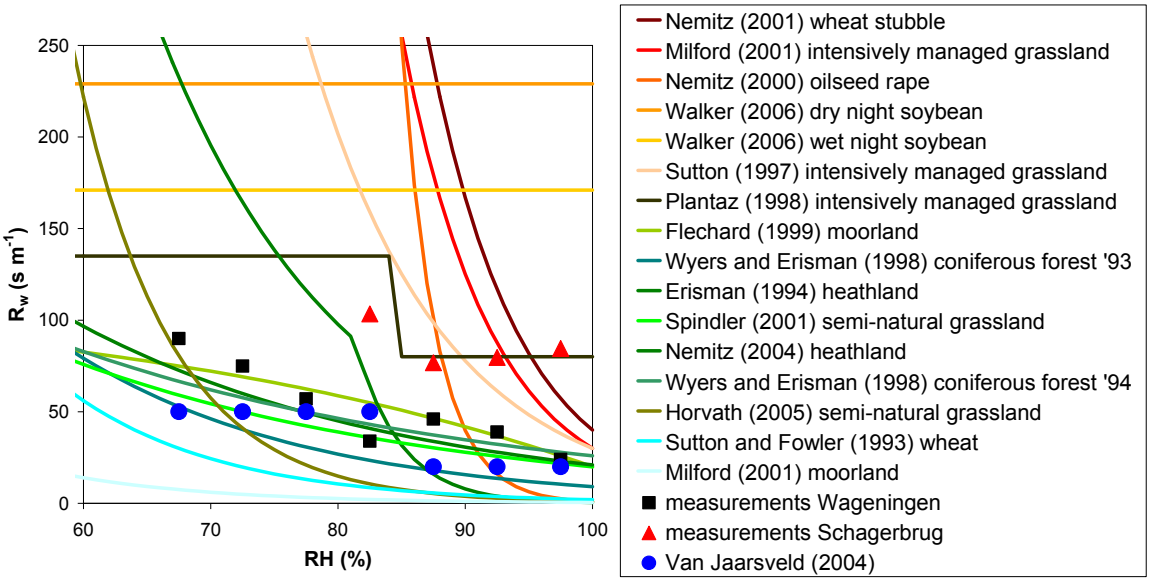

Figure 31. R_w versus relative humidity for 15 different flux measurement campaigns (represented by the coloured lines). The symbols represent 2 measurement campaigns over agricultural grassland in The Netherlands in Wageningen (non-fertilized; black squares) and Schagerbrug (fertilized; red triangles) and the current model parameterisation of Van Jaarsveld (2004) (blue circles).

For comparison, the harmonic averaged R_w values from the measurements over non-fertilized grassland site in Wageningen and the fertilized grassland site in Schagerbrug are included in this figure. We also included the paramaterisation of R_w in the DEPAC module (Appendix B) described in Van Jaarsveld (2004) that is used in the current version of the operational atmospheric transport model OPS of RIVM and PBL and the Lotos/Euros model of TNO, RIVM and PBL.
It is clear that in all studies, a lower relative humidity leads to a higher value of R_w. The same is true for higher ambient concentrations or pollution levels (increasing with line colours going from blue to green to red to brown). This conclusion is made based on the field studies in literature as well as on our own data. We see that R_w values for agricultural grassland (fertilized as well as non-fertilized) found in this study are much larger than the R_w values that are applied in the OPS model of RIVM for this land use class (Van Jaarsveld, 2004). An increase of R_w with increasing ambient concentration is also shown in a few other studies (Fowler et al., 1998; Jones et al., 2007). An explanation for this behaviour is that leaf water layers, which already exist at very low humidity (Van Hove et al., 1989), are getting

saturated. An update of the dry deposition description in the DEPAC module according to the current knowledge is therefore highly recommended.

Higher R_w values in the model will eventually result in lower deposition velocities and consequently higher air concentrations. It is shown that using the more realistic higher levels of R_w, 60% of the 'ammonia gap' can be explained (van Pul et al., 2008).

Literature

Baldocchi, D.D., Hicks, B.B., Camara, P., 1987. A canopy stomatal resistance model for gaseous deposition to vegetated surfaces. Atmospheric Environment - Part A General Topics 21, 91-101.

Beljaars A.C.M. and Holtslag A.A.M., 1991. Flux parameterization over land surface for atmospheric models. Journal of Applied Meteorology 30, 327–341.

Berkhout A.J.C., van der Hoff G.R., Bergwerff J.B., Swart D.P.J., Hensen A., Kraai A., Bleeker A., Huijsmans J.F.M., Mosquera J., van Pul W.A.J., 2008. Measuring ammonia emissions from manured fields. RIVM Report 6801500003/2008, Bilthoven, The Netherlands. 80pp.

Burkhardt, J., Gerchau, J., 1994. A new device for the study of water vapour condensation and gaseous deposition to plant surfaces and particle samples. Atmos Environ 28, 2012-2017.

Businger, J.A., Wyngaard, J.C., Izumi, Y., Bradley, E.F., 1971. Flux-profile relationships in the atmospheric surface layer. Journal of the Atmospheric Sciences 28, 181-189.

Davis, D.R., Hughes, J.E., 1970. A new approach to recording the wetting parameter by the use of electrical resistance sensors. Plant Disease Reporter 54, 474–479.

Dentener, F.J., Crutzen, P.J., 1994. A three-dimensional model of the global ammonia cycle. Journal of Atmospheric Chemistry 19, 331-369.

Derwent, R.G., Dollard, G.J., Metcalfe, S.E.,1988). On the nitrogen budget for the United Kingdom and north-west Europe. Quarterly Journal of the Royal Meteorological Society 114, 1127-1152.

Duyzer, J.H., Verhagen, H.L.M., Weststrate, J.H., Bosveld, F.C., Vermetten, A.W.M., 1994. The dry deposition of ammonia onto a Douglas fir forest in The Netherlands. Atmospheric Environment 28, 1241-1253.

Dyer, A.J., Hicks, B.B., 1970. Flux gradient relationships in the constant flux layer. Quarterly Journal of the Royal Meteorological Society 96, 715-721.

Dyer, A.J., 1974. A review of flux-profile relationships. Boundary-Layer Meteorology 7, 363-372.

Erisman, J.W., B.G. Van Elzakker, M.G. Mennen, J. Hogenkamp, E. Zwart, L. Vandenbeld, F.G. Romer, R. Bobbink, G. Heil, M. Raessen, J.H. Duyzer, H. Verhage, G.P. Wyers, R.P. Otjes, J.J. Mols, 1994. The Elspeetsche Veld Experiment on Surface Exchange of Trace Gases – Summary of Results, Atmospheric Environment 28, 487–496.

Flechard, C.R., Fowler, D., Sutton, M.A., Cape, J.N., 1999. A dynamic model of bi-directional ammonia exchange between semi-natural vegetation and the atmosphere. Quarterly Journal of the Royal Meteorological Society 125, 2611-2641.

Fowler, D., Pitcairn, C.E.R., Sutton, M.A., Flechard, C., Loubet, B., Coyle, M., Munro, R.C., 1998. The mass budget of atmospheric ammonia in woodland within 1 km of livestock buildings. Environmental Pollution 102, 343–348.

Gash, J.H.C., 1986. A note on estimating the effect of a limited fetch on micrometeorological evaporation measurements. Boundary-Layer Meteorology 35, 409-413.

Gillespie, T.J., Kidd, G.E., 1978. Sensing duration of leaf moisture retention using electrical impedance grids. Canadian Journal of Plant Science 58, 179–187.

Grennfelt, P., Hov, Ø., Derwent, R.G.,1994. Second generation abatement strategies for NOx, NH3, SO2 and VOC. Ambio 23, 425-433.

Holtslag, A.A.M., Van Ulden, A.P., 1983. A simple scheme for daytime estimates of the surface fluxes from routine weather data. Journal of Climate and Applied Meteorology 22, 517-529.

Horvath, L., Asztalos, M., Fuhrer, E., Meszaros, R., Weidinger, T., 2005. Measurement of ammonia exchange over grassland in the Hungarian Great Plain. Agricultural and Forest Meteorology 130, 282-298.

Jakobsen, H.A., J.E. Jonson, E. Berge, 1997. The multi-layer Eulerian model: Model description and evaluation of transboundary fluxes of sulphur and nitrogen for one year, EMEP/MSC-W Report 2/97, EMEP/Meteorological Synthesizing Centre - West, The Norwegian Meteorological Institute, Oslo, 1997.

Jones, M.R., I.D. Leith, D. Fowler, J.A. Raven, M.A. Sutton, E. Nemitz, J.N. Cape, L.J. Sheppard, R.I. Smith, M.R. Theobald, 2007. Concentration-dependent NH3 deposition processes for mixed moorland semi-natural vegetation. Atmospheric Environment 41, 2049–2060.

Mennen, M.G., Van Elzakker, B.G., Van Putten, E.M., Uiterwijk, J.W., Regts, T.A., Van Hellemond, J., 1996. Evaluation of automatic ammonia monitors for application in an air quality monitoring network. Atmospheric Environment 30, 3239-3256.

Milford, C., Theobald, M.R., Nemitz, E., Sutton, M.A., 2001. Dynamics of ammonia exchange in response to cutting and fertilising in an intensively managed grassland. Water, Air and Soil Pollution: Focus 1. 167-176.

Milieubalans, 2007. Milieu- en Natuurplanbureau, Bilthoven, 216 pp.

Monteith J.L., Unsworth M.H, 1990. Principles of environmental physics 2nd edn. Edward Arnold, London, p 291.

Mosquera J., Hensen, A., Van den Bulk, W.C.M., Vermeulen, A.T., Erisman, J.W., 2001. Long term NH3 flux measurements above grasslands in the Netherlands. Comparison between an intensive and an extensive field. Water, Air, and Soil Pollution: Focus 1, 203–212.

Nemitz, E., Sutton, M.A., Schjoerring, J.K., Husted, S., Wyers, G.P., 2000. Resistance modelling of ammonia above oilseed rape. Agricultural and Forest Meteorology 105, 405-425.

Nemitz, E., Milford, C., Sutton, M.A., 2001. A two-layer canopy compensation point model for describing bi-directional biosphere-atmosphere exchange of ammonia. Quarterly Journal of the Royal Meteorological Society 127, 815-833.

Nemitz, E., Sutton, M.A., Wyers, G.P., Jongejan, P.A.C., 2004. Gas-particle interactions above a Dutch heathland: I. Surface exchange fluxes of NH3, SO2, HNO3 and HCl. Atmospheric Chemistry and Physics 4, 989-1005.

Nieuwstadt, F., 1978. The computation of the friction velocity u_* and the temperature scale T_* from temperature and wind velocity profiles by least-square methods. Boundary-Layer Meteorology 14, 235-246.

Paulson, C.A., 1970. The mathematical representation of wind speed and temperature profiles in the unstable atmospheric surface layer. Journal of Applied Meteorology 9. 857-861.

Plantaz, M.A.H.G., 1998. Surface/atmosphere exchange of ammonia over grazed pasture. PhD thesis. Wageningen University, Wageningen, The Netherlands. 199 pp.

Schuepp, P.H., Leclerc, M.Y., Macpherson, J.I., Desjardins, R.L. (1990) Footprint prediction of scalar fluxes from analytical solutions of the diffusion equation. Boundary-layer Met., 50, 353-373.

Spindler, G., Teichmann, U., Sutton, M.A., 2001. Ammonia dry deposition over grassland - micrometeorological flux-gradient measurements and bidirectional flux calculations using an inferential model. Quarterly Journal of the Royal Meteorological Society 127, 795-814.

Stull, R.B., 1988. An introduction to Boundary Layer Meteorology. Kluwer Academic Publishers, Dordrecht, The Netherlands. 670 pp.

Sutton, M.A., Fowler, D., 1993. A model for inferring bi-directional fluxes of ammonia over plant canopies. Pp. 179-182 in Proceedings of the WMO conference on the measurement and modelling of atmospheric composition changes including pollution transport. Sofia, Bulgaria, 4-8 October 1993. WMO/GAW (Global Atmosphere Watch) 91. World Meteorological Organization, Geneva, Switzerland.

Sutton, M.A., Milford, C., Dragosits, U., Singles, R., Fowler, D., Ross, C., Hill, R., Jarvis, S.C., Pain, B.F., Harrison, R., Moss, D., Webb, J., Espenhahn, S., Halliwell, C., Lee, D.S., Wyers, G.P., Hill, J., ApSimon, H.M., 1997. Gradients of atmospheric ammonia concentrations and deposition downwind of ammonia emissions: First results of the ADEPT Burrington Moor Experiment. Pp. 131-139 in Gaseous nitrogen emissions from grasslands. Eds S.C. Jarvis and B.F. Pain. CAB International, Oxford, UK.

Van Dijk, A., Moene, A.F., De Bruin, H.A.R., 2004. The principles of surface physics: theory, practice and description of the ECPACK library. Internal Report 2004/1, Meteorology and Air Quality Group, Wageningen University, Wageningen, The Netherlands. 99pp.

Van Hove, L.W.A., Adema, E.H., Vredenberg, W.J., Pieters, G.A., 1989. A study of the adsorption of NH3 and SO2 on leaf surfaces. Atmospheric Environment 23, 1479-1486.

Van Jaarsveld, J.A., 2004. The operational priority substances model – Description and validation of OPS-Pro 4.1. RIVM report 500045001, RIVM, Bilthoven, The Netherlands. 156pp.

Van Pul, W.A.J., Van den Broek, M.M.P., Volten, H., Van der Meulen, A., Berkhout, A.J.C., Van der Hoek, K.W., Wichink Kruit, R.J., Huijsmans, J.F.M., Van Jaarsveld, J.A., De Haan, B.J., Koelemeijer, R.B.A., 2008. Het ammoniakgat: onderzoek en duiding. RIVM report 680150002/2008, RIVM, Bilthoven, The Netherlands. 97pp.

Walker, J.T., Robarge, W.P., Wu, Y., Meyers, T.P., 2006. Measurement of bi-directional ammonia fluxes over soybean using the modified Bowen-ratio technique. Agricultural and Forest Meteorology 138, 54-68.

Webb, E.K., Pearman, G.I., Leuning, R., 1980. Correction of flux measurements for density effects due to heat and water vapour transfer. Quarterly Journal of the Royal Meteorological Society 106, 85-100.

Wei Y.Q., B.J. Bailey and B.C. Stenning, 1995: A wetness sensor for detecting condensation on tomato plants in greenhouses. Journal of Agricultural Engineering Research 61: 197-204.

Wesely, M.L., 1989. Parameterization of surface resistances to gaseous dry deposition in regional-scale numerical models. Atmospheric Environment 23, 1293-1304.

Wichink Kruit, R.J., Van Pul, W.A.J., Otjes, R.P., Hofschreuder, P., Jacobs, A.F.G., Holtslag, A.A.M., 2007. Ammonia fluxes and derived canopy compensation points over non-fertilized agricultural grassland in The Netherlands using the new gradient ammonia-high accuracy-monitor (GRAHAM). Atmospheric Environment 41, 1275-1287.

Wyers G.P., Otjes R.P., Slanina J., 1993. A continuous flow denuder for the measurement of ambient concentrations and surface fluxes of ammonia. Atmospheric Environment 27, 2085-2090.

Wyers, G.P., Erisman, J.W., 1998. Ammonia exchange over coniferous forest. Atmospheric Environment 32, 441-451.

Appendix A. Micrometeorological variables and instrumentation at the micro meteorological observatory 'Haarweg' in Wageningen, The Netherlands

Meteorological variable	Units	Instruments	Type & Specifications
dry (T_d) and wet bulb (T_w) temperature	°C	aspirated psychrometer	Home made
vapour pressure	Pa	derived from T_d and T_w	-
saturation vapour pressure	Pa	derived from T_d and T_w	-
relative humidity	%	derived from T_d and T_w	-
relative humidity	%	hair hygrometer	
temperature and relative humidity	°C %	thermo-Hygrometer	Vaisala
air pressure	kPa	air pressure sensor	
precipitation amount	mm	rain gauge	Mierij Meteo
precipitation duration	minutes	rain gauge	Thies
wind speed at 4 levels	m s^{-1}	cup anemometer	KNMI
wind direction	deg	wind vane	Wieringa type
short wave radiation	W m^{-2}	pyranometer	Kipp en Zonen CM11
long wave radiation	W m^{-2}	pyrgeometer	Kipp en Zonen CG1
net radiation	W m^{-2}	derived from short and long wave radiation	
sun shine duration	minutes	sunshine Sensor	Heany (Austria)
soil temperatures under: bare soil:-5,-10,-20 cm grass:-5,-10,-20,-50,-100 cm	°C	Pt 100	Pico Technology
soil heat flux	W m^{-2}	heat flux plates	TNO type: Wp 51
CO_2/H_2O-concentration	mol m^{-3}	CO_2/H_2O Gas Analyzer	Licor-7500
wind speed (orthogonal)	m s^{-1}	sonic anemometer	CSAT3
(virtual) temperature T_v	°C	sonic anemometer	CSAT3
leaf wetness	-	leaf wetness sensor	Campbell Scientific model 237

Appendix B. Cuticular resistance (R_w) parameterisation in the DEPAC module

In the parameterisation of R_w for NH_3, there is a distinction made in pollution climates represented by NH_3/SO_2 ratios classified as low, high and very low. The corresponding NH_3/SO_2 ratios are, however, not defined. In the present implementation of the OPS model the 'high' definition is applicable under all circumstances. Only this part of the parameterisation is described here.

- For temperatures below 0 °C: $R_w = 200$
- For the land-use classes, water, urban and desert: $R_w = 5 + 19257 \exp(-0.094\ RH)$
- For coniferous and deciduous forests:
  - dry conditions: $R_w = 25 + 19257 \exp(-0.094\ RH)$
  - global radiation > 300 W m-2: $R_w = -500$#
  - wet conditions: $R_w = 20$
- For grassland, arable land and other grassy areas:

Daytime:	Spring and summer (dry):	$R_w = 100$
	Spring and summer (wet):	$R_w = 20$
	Autumn and winter (dry):	$R_w = 50$
	Autumn and winter (wet):	$R_w = 20$
Nighttime:	Spring and summer (dry):	$R_w = 50$
	Spring and summer (wet):	$R_w = 20$
	Autumn and winter (dry):	$R_w = 100$
	Autumn and winter (wet):	$R_w = 20$

This condition suggests that there is an upward (emission) flux.

RIVM

National Institute
for Public Health
and the Environment

P.O. Box 1
3720 BA Bilthoven
The Netherlands
www.rivm.com